



## PAPER

View Article Online  
View Journal | View Issue



Cite this: *Energy Environ. Sci.*, 2023, 16, 1644

# An artificial leaf device built with earth-abundant materials for combined H<sub>2</sub> production and storage as formate with efficiency > 10%†

Claudio Ampelli, \*<sup>a</sup> Daniele Giusi, <sup>a</sup> Matteo Miceli, <sup>a</sup> Tsvetelina Merdzhanova, <sup>b</sup> Vladimir Smirnov, <sup>b</sup> Ugochi Chime, <sup>b</sup> Oleksandr Astakhov, <sup>b</sup> Antonio José Martín, <sup>c</sup> Florentine Louise Petronella Veenstra, <sup>c</sup> Felipe Andrés Garcés Pineda, <sup>d</sup> Jesús González-Cobos, <sup>‡</sup> Miguel García-Tecedor, <sup>§</sup> Sixto Giménez, <sup>e</sup> Wolfram Jaegermann, <sup>f</sup> Gabriele Centi, <sup>a</sup> Javier Pérez-Ramírez, <sup>c</sup> José Ramón Galán-Mascarós <sup>d</sup> and Siglinda Perathoner <sup>a</sup>

A major challenge for achieving energy transition and transforming the current energy model into distributed production is the development of efficient artificial leaf-type devices capable of directly converting carbon dioxide (CO<sub>2</sub>), water and sunlight into sustainable fuels and chemicals under ambient conditions. These devices should avoid using critical raw materials to be sustainable and cost-competitive. We report top-level results for the first time in converting CO<sub>2</sub> and H<sub>2</sub>O to fuels (formate and H<sub>2</sub>) using sunlight and electrodes based solely on earth-abundant materials. The cell provides a solar-to-fuel efficiency of >10% combined with world-record current densities to comparable devices operating at room temperature, without adding sacrificial donors or electrical bias. In addition, we present the novel concept of producing at the same time H<sub>2</sub> and an H<sub>2</sub>-storage element (formate), the latter used to produce H<sub>2</sub> when light is absent. This solution allows continuous (24 h) hydrogen production using an artificial-leaf device. For the first time, we show the feasibility of this solution. The experimental results were obtained in an optimised, compact electrochemical flow cell, with electrodes based on Cu–S and Ni–Fe–Zn oxide (for CO<sub>2</sub> reduction and oxygen evolution reactions, respectively) supported on gas-diffusion substrates, integrated with a low-cost Si-based photovoltaic module. The cell design allows for easy scale-up and low manufacturing and operating costs. The cell operates at a current density of about 17 mA cm<sup>−2</sup> and a full-cell voltage of 2.5 V (stable for at least ten hours and in on–off operations), providing formate productivity of 193 μmol h<sup>−1</sup> cm<sup>−2</sup>, paving the way towards the implementation of affordable artificial-leaf type systems in the future energy scenario.

Received 4th October 2022,  
Accepted 14th February 2023

DOI: 10.1039/d2ee03215e

rsc.li/ees

<sup>a</sup> Department of Chemical, Biological, Pharmaceutical and Environmental Sciences (ChiBioFarAm), University of Messina, ERIC aisbl and CASPE/INSTM, Messina, Italy.  
E-mail: ampellic@unime.it

<sup>b</sup> IEK5-Photovoltaik, Forschungszentrum Jülich GmbH, 52425 Jülich, Germany

<sup>c</sup> Institute for Chemical and Bioengineering, Department of Chemistry and Applied Biosciences, ETH Zürich, Vladimir-Prelog-Weg 1, 8093 Zürich, Switzerland

<sup>d</sup> Institute of Chemical Research of Catalonia (ICIQ), The Barcelona Institute of Science and Technology (BIST), Av. Paisos Catalans 16, 43007 Tarragona, Spain

<sup>e</sup> Institute of Advanced Materials (INAM), Universitat Jaume I, Castelló, Spain

<sup>f</sup> Technical University of Darmstadt, 64287 Darmstadt, Germany

† Electronic supplementary information (ESI) available. See DOI: <https://doi.org/10.1039/d2ee03215e>

‡ Present address: Institut de Recherches sur la Catalyse et l'Environnement de Lyon, UMR 5256, CNRS, Université Claude Bernard Lyon 1, 2 Avenue A. Einstein, 69626 Villeurbanne, France.

§ Present address: Photoactivated Processes Unit, IMDEA Energy, Avda. Ramón de la Sagra, 3, 28935 Móstoles, Spain.



### Broader context

Developing artificial leaves to directly convert CO<sub>2</sub>, H<sub>2</sub>O and sunlight into valuable fuels and chemicals (by mimicking the behaviour of plants in nature) is one of the fascinating challenges to face in the energy transition. However, artificial leaves or photosynthesis technology is still considered a long-term objective due to limitations such as expensive materials, low robustness and poor performance. We have demonstrated in this study that it is possible to construct artificial-leaf devices that reach a solar-to-fuel efficiency of 10% (still considered a long-term target in the area) using easily scalable systems with no critical raw materials, operating under mild conditions and without adding sacrificial donors or electrical biases. This study proves the concept of manufacturing on a lab scale an artificial leaf made with only earth-abundant materials with stable operations until at least 10 h of light irradiation and with performance among the highest values reported in the literature in terms of current density and solar-to-fuel efficiency. At the same time, we demonstrate the proof of concept of another challenge: how to produce with continuity (all day) hydrogen in a device using sunlight. We have developed an artificial-leaf device that integrates the chemical hydrogen storage as formate, which can produce H<sub>2</sub> again during dark periods. The new artificial leaf produces formate with high C-selectivity and hydrogen. Formate is one of the most promising liquid energy carriers working under ambient conditions, showing potential as a hydrogen carrier for the new hydrogen economy. The combination of formate and H<sub>2</sub> production is thus proposed here for the first time as a new solution for the continuous daily production of hydrogen.

## 1 Introduction

Artificial photosynthesis to convert carbon dioxide (CO<sub>2</sub>) and water directly into value-added chemicals is one of today's challenges to meet growing energy demands and curb climate changes due to the accumulation of CO<sub>2</sub> in the environment.<sup>1–3</sup> Artificial leaves (ALs) are small-scale reactors involving the electrocatalytic transformation of abundant small molecules (*i.e.*, water, carbon dioxide, dinitrogen, and methane) using renewable sources such as solar power.<sup>4</sup> ALs can have different configurations: (i) a wired or wireless configuration,<sup>5</sup> with the photoactive element in contact with the electrolyte or (ii) a configuration where the photoactive element (a photovoltaic – PV – cell) is not in contact with the electrolyte, although integrated into the device. This second configuration is preferable for stability and performance.<sup>3</sup> To be sustainable, ALs should be manufactured using earth-abundant materials.<sup>5,6</sup> It is also crucial to adopt cell engineering and design suitable for easy scale-up and mass production,<sup>3</sup> avoiding using sacrificial donors or electrical bias.<sup>7</sup> Stability is another critical requirement, which implies using stable materials, and cell design and operating conditions enabling long-term operations.

Hydrogen (H<sub>2</sub>) is considered the simplest fuel generated from an AL. Khaselev and Turner already studied direct water electrolysis in 1998. They reported an integrated-monolithic photoelectrochemical-photovoltaic device with 12.4% hydrogen efficiency at 11 Suns of light irradiation using rare earth elements to prepare electrodes (*i.e.*, GaInP<sub>2</sub>/GaAs).<sup>8</sup> Another pioneering device for artificial photosynthesis was the cell introduced by Nocera's group over ten years later, unveiling the first practical artificial leaf (working at one SUN under near-neutral pH conditions) for water splitting with 5% solar efficiency.<sup>9</sup> This cell was made of cheap materials but can only be used for hydrogen production. In addition, severe stability issues were present due to photo corrosion of the integrated PV cell in contact with the electrolyte.

ALs producing higher energy-density fuels by converting CO<sub>2</sub> into C-containing products (allowing closing of the cycle of CO<sub>2</sub> formation/consumption) are an alternative and more attractive solution than water-splitting devices that produce H<sub>2</sub>, with

the benefits of generating “drop-in” carbon fuels ready to be introduced into the current energy infrastructure.<sup>10</sup> The most common carbon fuels/chemicals formed by (photo-) electrocatalytic (PEC) reduction of CO<sub>2</sub> include carbon monoxide (CO), formate (HCOO<sup>−</sup>), methanol (CH<sub>3</sub>OH), ethylene (C<sub>2</sub>H<sub>4</sub>), and other C<sub>2</sub>+ alcohols, hydrocarbons, and acids (where C<sub>2</sub>+ refers to products with two or more carbon atoms). However, carbon monoxide<sup>11</sup> and formate,<sup>12</sup> formed by two electron reduction of CO<sub>2</sub>, have so far been the only carbon products generated with high Faradaic efficiency (FE) at relevant current densities (> 10 mA cm<sup>−2</sup>). Carbon monoxide requires further processing with H<sub>2</sub> to produce fuels or chemicals. Formate is instead the base material for several industries and is a highly desirable product.<sup>13,14</sup> It can also act as an energy carrier for direct formate fuel cells, for example, or as an H<sub>2</sub>-carrier. Formate has a high volumetric H<sub>2</sub> storage capacity of 53 g<sub>H<sub>2</sub></sub> L<sup>−1</sup>,<sup>15</sup> and low toxicity and flammability for low-cost hydrogen storage and transportation.

From this perspective, the combined production of formate and H<sub>2</sub> in an efficient AL-type device is an attractive solution because it can produce at the same time green H<sub>2</sub>, and a hydrogen carrier easy to store. Such a device can be integrated into distributed networks of green H<sub>2</sub>, with fluctuations in H<sub>2</sub> production due to sunlight variability mitigated by the use of the hydrogen carrier. CO<sub>2</sub> can then be closed-up by recirculating it.

This solution presents advantages over the combinations of PV, wind, and electrical energy storage (batteries), eventually coupled with water electrolyzers to produce H<sub>2</sub> continuously. The chemical energy storage has a volumetric energy density about three orders of magnitude greater. Realising a distributed approach of many parallel devices (artificial trees) would require enough compact artificial leaf devices and thus explore chemical storage as an alternative to electrochemical storage. It is possible to imagine an artificial tree that produces H<sub>2</sub> and integrates the storage of H<sub>2</sub> as formate to produce on-demand H<sub>2</sub> during dark periods.

However, it is a largely unexplored option, still lacking available devices with suitable characteristics for this technology. In this sense, the combined and balanced production of formate



and H<sub>2</sub> with high solar-to-fuel efficiency is the target, rather than obtaining a high FE to formate. However, the C-selectivity to formate, *i.e.*, the selectivity of converting CO<sub>2</sub> to formate rather than other C-products such as CO, methanol and higher alcohols, hydrocarbons, *etc.*, is required.

One of the most recent PEC approaches for selective formate generation was developed by Domen's group, reporting a scalable CO<sub>2</sub> reduction process using a molecular-based hybrid photocatalyst with a remarkable selectivity to formate ( $97 \pm 3\%$ ).<sup>16</sup> However, critical raw materials were used for the preparation of electrodes (*i.e.*, SrTiO<sub>3</sub>:La, Rh) and a very low solar-to-formate efficiency was obtained ( $0.08 \pm 0.01\%$ ).

In 2016, Zhou *et al.* reported a high 10% energy-conversion efficiency with a current density of about 9 mA cm<sup>-2</sup> but using a costly InGaP/GaAs PV component, a noble metal-based cathode with a very small electrode surface area (0.03 cm<sup>2</sup>), *i.e.* not suited to analyse scalability to large-scale application.<sup>17</sup> Furthermore, Piao *et al.* reported an overall solar conversion efficiency of about 8.5% with a current density of about 10 mA cm<sup>-2</sup> but using expensive electrodes (*i.e.*, IrO<sub>2</sub> as the anode) and a chlorite-promoted electrolyte (with corrosion and safety issues for the possible formation of Cl<sub>2</sub>).<sup>18</sup> Recently, Kato *et al.*<sup>19</sup> reported a solar-driven electrochemical reduction of CO<sub>2</sub> to formate with a conversion efficiency of 7.2% using a Si-based PV cell, then scaled up to 1 m<sup>2</sup> eight-stacked electrodes with an improved efficiency of 10.5%,<sup>20</sup> but also, in this case, costly noble-metal based electrodes (anodes based on IrO<sub>x</sub> and cathodes on a molecular Ru-complex polymer) were used. In summary, examples of efficient artificial-leaf-type devices free of noble metals or expensive materials have not been reported so far for formate production at a relatively high current density, nor has the balanced coproduction of formate and H<sub>2</sub> been investigated. Coproducing H<sub>2</sub> and an H<sub>2</sub>-storage element, which can produce H<sub>2</sub> during dark periods, is a novel possibility opening breakthrough research directions.

In this study, we present the realisation of a lab-scale bias-free PV/EC flow cell for converting CO<sub>2</sub> and water into formate and H<sub>2</sub> (and O<sub>2</sub>) under sunlight irradiation (one SUN), using only earth-abundant materials for device construction. The PV/EC architecture generally indicates a photovoltaic (PV) module integrated within the electrochemical (EC) cell but not in contact with the electrolyte to enable high stability of the PV component. In PEC (photo-electro-catalytic) cells, instead, the PV unit is in direct contact with the electrolyte or a semiconductor-based photoelectrode is used. A survey of state-of-the-art results indicates that the PV/EC architecture is currently preferable.<sup>21</sup>

Our PV/EC cell, working as an AL-type device at room temperature and atmospheric pressure, has a highly compact design, amenable to scale-up, and is integrated with gas diffusion electrodes based on Cu-S for CO<sub>2</sub> reduction and Ni-Fe-Zn oxide for water oxidation. The electrochemical (EC) part is coupled with a low-cost PV four-cell module with shingled interconnection based on the silicon heterojunction (SHJ) technology, leading to a full lab-scale prototype that delivers outstanding performance by converting over 6% of sunlight

into carbon fuels (with high selectivity to formate), and delivers an overall 10% solar-to-fuel efficiency also including hydrogen production. Formate is accumulated in the liquid phase located at the EC part and separated from the gas outlet rich in H<sub>2</sub>. Formate can then be recovered from the electrolyte without using energy-intensive separation solutions,<sup>22</sup> or stored and then decomposed (to produce H<sub>2</sub>) without the need to be separated from the electrolyte.

The realisation of the combined PV/EC device is the result of optimisation of many aspects in relation to:

- (i) operating close to the maximum power point of the PV device;
- (ii) reaching a cell voltage in the EC device high enough to drive the reduction/oxidation reactions;
- (iii) minimising energy losses due to overpotential;
- (iv) controlling potentials within the stability limits of the catalysts.

This artificial leaf-type system was developed within a European project (A-LEAF) dedicated to realising a prototype from earth-abundant materials for sustainable solar production of CO<sub>2</sub>-based chemicals and fuels.<sup>23</sup> In this project, the integrated development of the photoactive element, the electrocatalysts, the electrodes and the cell was studied. The results of this study show that the optimal behaviour does not derive from the independent optimisation of the separated elements. Rather, an integrated (combined) development is necessary. This manuscript reports the results of this integrated effort combining scientific advances in materials with the identification of the limiting aspects that determine the overall behaviour and the way to overcome them.

## 2 Description of the device

Fig. 1 schematically illustrates our AL-type device and its components. The device is composed of two main parts: (i) a two-compartment electrochemical (EC) cell and (ii) a photovoltaic (PV) module, combined in a single PV/EC unit to minimise energy losses and operate at maximum performance.

The following subsections describe the EC cell and PV module.

### 2.1 Electrochemical cell

The EC cell is a lab-scale device made of Plexiglas (a transparent material for an easy visual inspection of what happens inside), working as an electrochemical flow cell with optimised pathways for gas and liquid flows. An exploded view of the artificial leaf shows details of the main elements of the EC cell (see Fig. 1a).

A gas diffusion layer (GDL) separates a gas chamber (directly fed with pure CO<sub>2</sub>) from the liquid catholyte (0.1 M KHCO<sub>3</sub> aqueous solution saturated with CO<sub>2</sub>, pH 6.8). The active catalytic material for CO<sub>2</sub> reduction (*i.e.*, Cu-S) faces the electrode side towards the liquid part. The gas diffusion electrode –GDE– (in combination with the gas chamber) facilitates an efficient gas-liquid contact in the proximity of



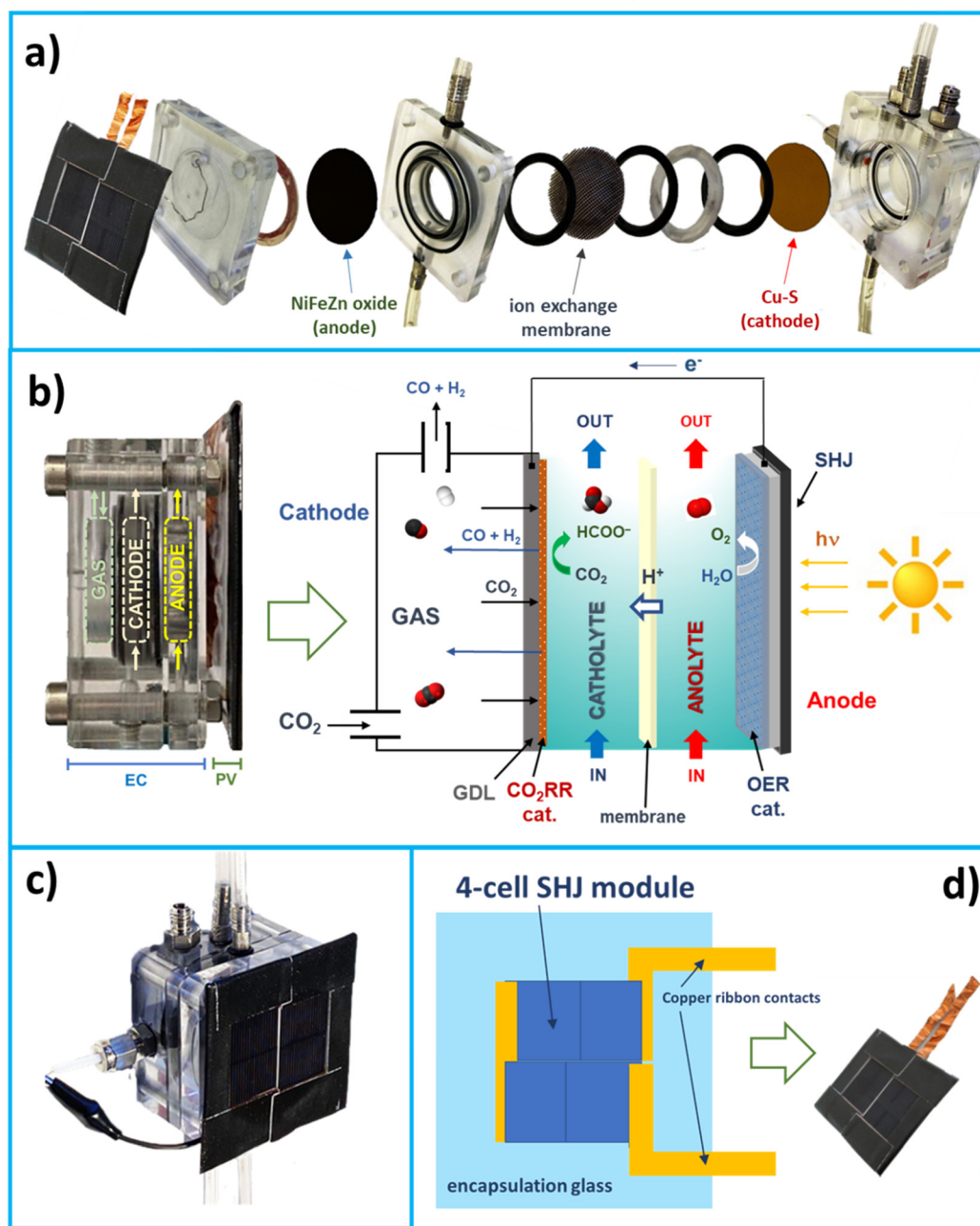


**Fig. 1** Visual description of the artificial leaf and its elements. (a) Exploded view of the electrochemical (EC) – photovoltaic (PV) device and related electrodes, including O-rings and rubbers; (b) representative scheme of the working principle of the artificial leaf (a side picture is also provided on the left). The  $\text{CO}_2$  Reduction Reaction ( $\text{CO}_2\text{RR}$ ) occurs in a liquid electrolyte (catholyte) at the cathode side. A gas chamber enhances the local concentration of gaseous  $\text{CO}_2$  (directly on the electrode surface) flowing through a Gas Diffusion Layer (GDL). The counter-reaction is the Oxygen Evolution Reaction (OER) by water oxidation. "cat." represents catalyst; (c) picture of the full PV/EC device; and (d) scheme and picture of the silicon heterojunction (SHJ) four-cell module used to absorb sunlight and provide electricity.

the electrode, improving the transport of gaseous species through the carbon fibre support due to hydrophobic repulsion with the liquid phase.<sup>24</sup> The counter anodic process is the Oxygen Evolution Reaction (OER) occurring over a Ni–Fe–Zn oxide-based electrode in 1 M KOH aqueous solution ( $\text{pH} \approx 14$ ).

The use of two different electrolytes in the cathode and anode compartments is due to the individual optimisation of

the electrocatalytic performance of Cu–S and Ni–Fe–Zn oxide, respectively, occurring at different pHs, as well as due to the stability of the electrodes under these conditions to the working potential (see Sections S1 and S2 in the ESI†). Using a commercial proton exchange membrane (*i.e.*, PTFE-reinforced Nafion) allowed keeping this pH difference during the electrocatalytic tests, providing an optimal charge transfer between catholyte and anolyte liquids and limiting crossover of





intermediate/product species. The choice of the best membrane was accomplished by selecting among a series of commercial cationic, anionic and bipolar membranes with different characteristics (see Section S3 in the ESI† for further details).

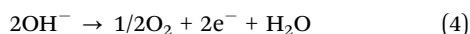
The EC cell was designed in a highly compact configuration following general criteria to minimise overpotentials and resistances (e.g., short distance between the electrodes; optimisation of electrolyte volumes), supported by preliminary experimental tests to verify the origin of internal energy losses (see Section S4 in the ESI†).

Careful optimisation of gas and liquid flows was demanded to guarantee a proper diffusion of CO<sub>2</sub> through the GDL and avoid liquid leaks in the gas chamber. Catholyte and anolyte were continuously recirculated between each half-cell and two reservoirs. Fig. 1b reports a representative scheme showing the working principle of the artificial leaf, while Fig. 1c shows a picture of the full prototype. We also included a short video in the ESI† to show the artificial leaf during its regular operation.

The half-reactions occurring at the cathode side refer to CO<sub>2</sub> reduction to formate and CO (eqn (1) and (2)), and proton reduction to produce H<sub>2</sub> (eqn (3)), reported as follows:



while at the anode side, the OER takes place:



Note that the gas products obtained from reactions (2) and (3) (CO and H<sub>2</sub>, respectively) are collected in full from the outlet of the gas chamber (diffusing back through the GDL), and do not dissolve in the liquid catholyte, as the gas chamber operates at atmospheric pressure.<sup>25</sup>

## 2.2 Photovoltaic module

We used a mini-PV device composed of four silicon heterojunction solar cells,<sup>26</sup> with an area of 12.71 cm<sup>2</sup>, interconnected in a shingled configuration<sup>27</sup> and encapsulated using a glass/thermoplastic polyolefin (TPO)/module/TPO/back sheet structure<sup>28</sup> (see Fig. 1d). The PV module is located externally close to the anode side of the EC cell (not in contact with the liquid anolyte) and connected with short electrical wires to the EC part. The solar PV module absorbs sunlight and provides electricity needed for the electrocatalytic processes.

# 3. Results and discussion

## 3.1 Electrocatalysts and electrodes

The cathode is made of sulphur-modified copper oxide (Cu-S), synthesised by the solvothermal method. The synthesis and optimisation of Cu-S were earlier reported by Shinagawa *et al.*,<sup>29</sup> along with its performance in the electrocatalytic CO<sub>2</sub> reduction reaction. However, the synthesis of Cu-S was up-

scaled for the preparation of technical electrodes to be used in an integrated PV/EC device under relevant conditions.

Copper-based systems are affordable and earth-abundant catalysts for the (photo-)electro-reduction of CO<sub>2</sub> into various compounds ranging from C1 to C3 with appreciably Faradaic efficiencies.<sup>30,31</sup> To deliver a single liquid carbon product and thus avoid downstream separation needs, sulphur-modified copper oxide (Cu-S) was the catalyst of choice because of its scalable preparation (see details in the experimental part section) and total selectivity towards formate among carbon products.<sup>29</sup> The surface modification of copper systems with small amounts of sulphur (0.45 at% content in this work) suppresses routes initiated by CO adsorption, thus avoiding its formation and that of more complex compounds.

The fresh catalyst contains polycrystalline Cu<sub>2</sub>O displaying a homogeneous sulphur distribution (Fig. 2a), where CuS and CuS<sub>2</sub> domains could be identified by selected area electron diffraction (SAED) analysis (Fig. 2b). Cu-S systems undergo reconstruction under operating conditions leading to a stable sulphur-enriched Cu surface responsible for the preference towards formate of these systems, as reported elsewhere.<sup>29</sup>

Cu-S was finally deposited on a commercial GDL by spray coating (1 mg cm<sup>-2</sup> loading) to facilitate gas transport of reagents (CO<sub>2</sub>) and gaseous products (CO and H<sub>2</sub>).

The anodic material is Ni-Fe-Zn oxide, obtained by hydrothermal methods in water (more details are provided in the experimental section), then deposited on a commercial GDL to prepare the electrode (1 mg cm<sup>-2</sup> loading) and facilitate O<sub>2</sub> desorption.

Ni-Fe-Zn oxide shows outstanding performance during the OER in alkaline media. This oxide interestingly improved its electrocatalytic behaviour during accelerated stability tests compared to the as-prepared oxide (see Section S5 in the ESI†), as also confirmed and reported earlier.<sup>32</sup>

Nanoparticles with narrow-distribution sizes (8–10 nm) were obtained, identified as a spinel system with a space group of *Fd3m*. This mixed metallic oxide exhibited high stability, retaining its structure after long-term periods of polarisation at a potential higher than 1.5 V vs. RHE with only minimal Zn<sup>2+</sup> leaching (see Section S5 in the ESI†), responsible for the increased electrochemically active surface area during operation. The electron microscopy analyses confirmed the robustness of this oxide. The images shown in Fig. 2c–e refer to the Ni-Fe-Zn oxide after the electrocatalytic tests, evidencing no substantial differences from the as-prepared oxide (before electrolysis) as reported in Section S5 in the ESI†.

## 3.2 Electrocatalytic performance in a three-electrode configuration

The electrochemical testing (without solar irradiation) was first carried out in the compact EC device described above by adopting a three-electrode configuration and applying an electrical bias to the cathode from −0.4 to −1.0 V vs. RHE. A very thin capillary Ag/AgCl (3 M KCl) electrode was used as the reference electrode and placed very close to the Cu-S/GDL.



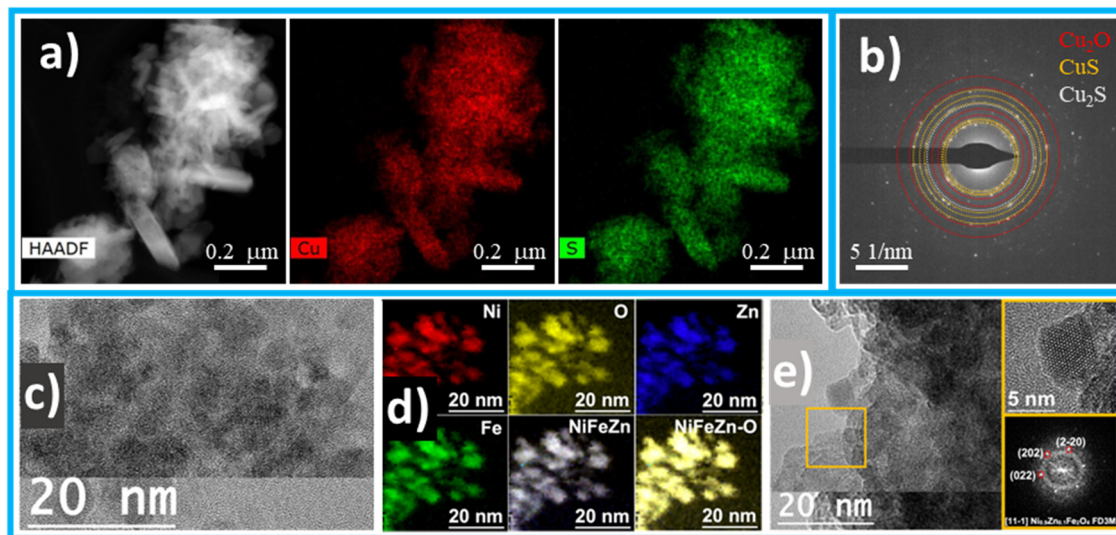


**Fig. 2** Characterisation of electrocatalytic materials. For the cathodic Cu–S catalyst: (a) representative scanning transmission electron microscopy (STEM) image in the high-angle annular dark field (HAADF) and corresponding elemental maps obtained by energy-dispersive X-ray spectroscopy (EDX); and (b) selected area electron diffraction (SAED) showing the presence of sulphide phases. A more detailed characterisation can be found in ref. 29. For the anodic NiFeZn oxide catalyst (after electrolysis): (c) HAADF STEM micrograph of the Ni–Fe–Zn nanoblock sample; (d) EELS chemical composition maps obtained of the STEM micrograph, showing individual Ni L<sub>2,3</sub>-edges at 855 eV (red), Fe L<sub>2,3</sub>-edges at 708 eV (green), Zn L<sub>2,3</sub>-edges at 1020 eV (blue) and O K-edge at 532 eV (yellow) as well as composites of NiFeZn and NiFeZn–O; and (e) high-resolution transmission electron microscopy (HRTEM) image taken from an agglomerate nanoparticle squared in orange. Details of the orange squared region and its corresponding power spectrum reveal that this nanoparticle has a crystal phase in agreement with the Ni<sub>0.9</sub>Zn<sub>0.1</sub>Fe<sub>2</sub>O<sub>4</sub> cubic phase (space group = *FD3M*) with *a* = *b* = *c* = 8.3540 Å. From the crystalline domain in the inset, the Ni<sub>0.9</sub>Zn<sub>0.1</sub>Fe<sub>2</sub>O<sub>4</sub> lattice fringe distances are measured to be 0.294 nm, 0.292 nm and 0.295 nm, at 60.64° and 121.06°, which could be interpreted as the cubic Ni<sub>0.9</sub>Zn<sub>0.1</sub>Fe<sub>2</sub>O<sub>4</sub> phase, visualised along its [11-1] zone axis. The characterization of the as-prepared NiFeZn oxide catalyst (before electrolysis) is reported in Section S5 in the ESI†

The adopted EC design is quite different from the conventional electrochemical setups (e.g., the H-type configuration) in which an electrocatalytic substrate is immersed in a liquid electrolyte. Our compact prototype shows many advantages, such as (i) low energy loss (due to the compact cell configuration); (ii) high local concentration of CO<sub>2</sub> on the electrode surface (due to the combined use of a GDE with a gas chamber for a direct feed of CO<sub>2</sub> through the GDL); and (iii) easy scale-up to higher geometrical surface areas. While liquid products from CO<sub>2</sub> reduction (*i.e.*, formate) are separately collected in the catholyte and sampled from the external cathode reservoir for the analysis, the gas products diffuse back through the GDE and exit from the gas-chamber outlet (see Fig. 1b). To confirm the pathway of gas products, we checked out the absence of CO and H<sub>2</sub> in the headspace of the cathode reservoir.

An accurate, standardised protocol, consisting of a series of Cyclic Voltammetry (CV) analyses to stabilise the electrodes and to measure the capacitance before and after each test, was strictly followed (more details are reported in Section S6 in the ESI†).

A series of preliminary blank tests were also performed to verify that formate derives from the CO<sub>2</sub> feed to the PV/EC cell. A standard procedure was to feed an inert gas rather than CO<sub>2</sub> and monitor whether carbon products were formed during these tests.

Fig. 3a shows the results obtained from the electrochemical testing. The FE to formate (see the green bars) increases with

the applied voltage reaching a maximum value of 62.2% at −1.0 V and 15.1 mA cm<sup>−2</sup>. In contrast, the FE to hydrogen decreases by increasing the voltage. At −1.0 V, carbon monoxide also forms (FE to CO is 4.2%). Thus, the voltage at the working electrode (cathode) should not overcome −1.0 V to maximise the carbon selectivity towards formate and avoid costs in downstream gas separation. Fig. 3b shows the results of a further validation test performed in a galvanostatic mode by applying a constant current density (10 mA cm<sup>−2</sup>) and measuring the working and cell voltages. A steady-state value of 2.5 V was reached for the cell voltage (difference between working and counter voltages), evidencing quite good stabilisation in 1 hour and a half. These electrochemical tests provided relevant information to set the operating conditions of the artificial leaf and select the PV module suitable for coupling.

Table 1 summarises the specifications of the main components of the EC device.

### 3.3 PV module and coupling

As indicated in the introduction, rather than decorating PV cells with electrocatalytic materials in a “wireless” configuration<sup>33–35</sup> (with all the intrinsic limits of stability and photo corrosion), we opted to a PV/EC configuration, with the PV module not in contact with the electrolyte, to enhance stability of operation but also to flexibly change the PV module. Our device incorporates an external PV module wired to the EC cell to reach the required photo potential for both half-cell reactions, thus avoiding the



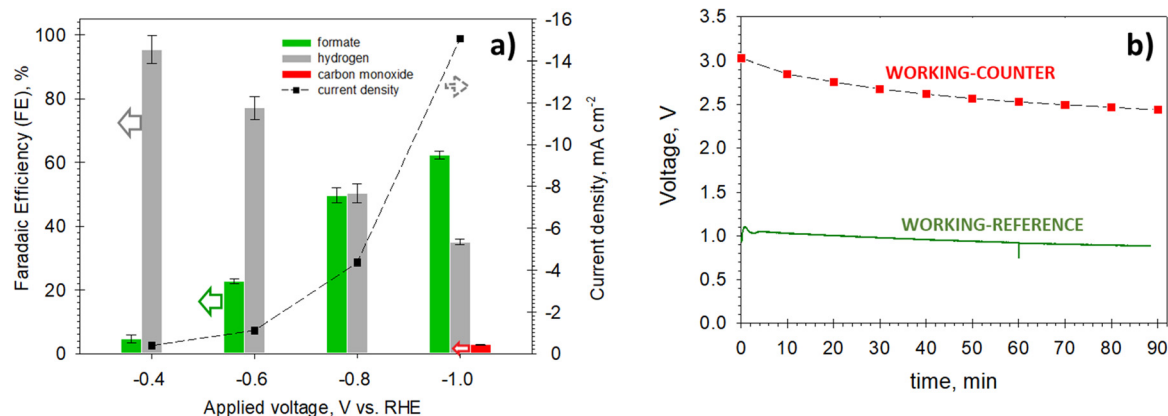


Fig. 3 Performances of the electrochemical device. (a) Faradaic efficiency (FE) from electrochemical tests at a different applied voltage (vs. RHE) in a three-electrode configuration. The measured current density profile is also reported. (b) Working-counter (cell voltage) and working-reference (vs. RHE) voltage profiles versus time obtained by an electrochemical test at 10 mA cm<sup>-2</sup>.

Table 1 Specifications of the main components of the electrochemical EC device

Cathode	Cu-S/GDL (1.0 mg cm <sup>-2</sup> )
Anode	Ni-Fe-Zn oxide/GDL (1.0 mg cm <sup>-2</sup> )
Catholyte	0.1 M KHCO <sub>3</sub> aqueous solution saturated with CO <sub>2</sub> (pH = 6.8)
Anolyte	1 M KOH aqueous solution (pH > 13)
Membrane	Nafion™ N324, Teflon™ Fabric Reinforced
Reference electrode	3 M KCl Ag/AgCl (1 mm dia.)

inevitable decrease in performance due to charge recombination effects at the interface.

The 4-cell SHJ module, described in Section 2.2, was designed and realised to match the EC cell's characteristics and size. The current-voltage (*I*-*V*) characteristics and the PV parameters of the 4-cell SHJ module are reported in Section S9 in the ESI†. Under these conditions, the PV module provides 20.3% conversion efficiency at the maximum power point (MPP).

The coupling procedure between EC and PV was performed using a Xe arc-lamp of 300 W equipped with an Air-Mass 1.5 Global filter. The PV module was calibrated to operate at 1 SUN (100 mW cm<sup>-2</sup>) by accurately setting the distance from the lamp and the opening of the diaphragm (see Section S10 in the ESI†). Under real operating conditions (without cooling of the PV module), the measured temperature was slightly higher than 25 °C (*i.e.*, 31.5 °C), reducing the conversion efficiency of the PV module from 20.3 to 19.74%.

After the preliminary tests on the whole integrated PV/EC system, we refined the design of the EC cell. We manufactured a more compact cell (further reducing the volume of both liquid compartments and the distance between the electrodes) to reach a cell voltage of 2.5 V at the operating point and stay as close as possible to the MPP of the PV module. The resulting combination of the two polarisation curves of EC and PV is shown in Fig. 4.

The EC polarisation curve reported on the graph was constructed by varying the applied voltage at the working electrode and measuring both current and cell voltage after about 30 min

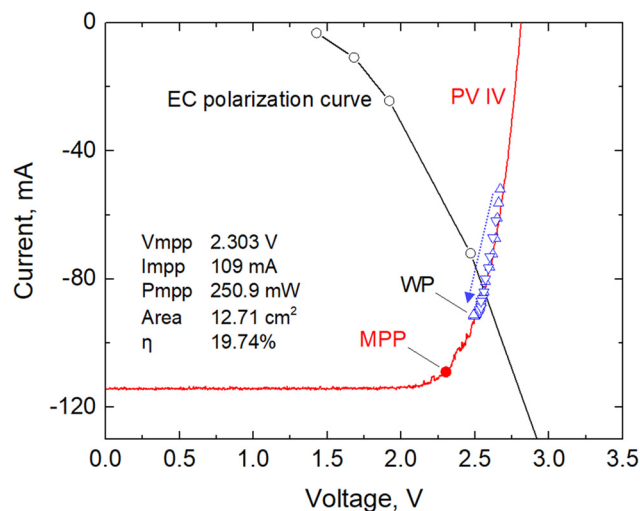


Fig. 4 Coupling of the photovoltaic module with the electrochemical device. The *IV* curve of the SHJ photovoltaic (PV) module and the polarisation curve of the electrochemical (EC) cells are plotted together. The working point (WP) of the artificial leaf and the maximum power point (MPP) of the PV module are also indicated on the plot (at a cell voltage of 2.5 V and 2.3 V, respectively). The blue triangles indicate the evolution of the WPs (in the direction indicated by the arrow) during the 10 h validation test.

of operation (needed to stabilise the signal). The point of intersection between the two curves (*i.e.*, 2.6 V) should indicate the artificial leaf's working point (WP). However, the electrochemical behaviour of the EC cell is quite dynamic, mainly due to the evolution of the electrocatalysts, especially in the first 2–3 h of the reaction. During the stability validation test of 10 h, we thus investigated the evolution of the WP, which stabilised at a cell voltage of 2.5 V (in line with the electrochemical tests performed with only the EC device), as will be discussed in the next section.

### 3.4 Validation of the device

The coupled PV/EC device was validated under certified standard conditions of solar irradiation (AM1.5 G, 1 SUN, 100 mW cm<sup>-2</sup>),



working in a two-electrode configuration (without a reference electrode).

Note that the electrodes were made with earth-abundant materials (Cu, Ni, Fe, Zn, and C), and neither electrical bias nor sacrificial donors were added. The latter means that the energy needed for running the electrochemical reactions ( $\text{CO}_2$  reduction at the cathode and water oxidation at the anode) only originates from the solar simulator.

The AL-type device was validated in two series of 5 h photo-electrochemical tests (10 h in total). These tests indicate the robustness and stability of the device, as well as the performance recovery after on-off operations. After the first five hours, light irradiation was stopped, and the anolyte and catholyte (the latter containing the  $\text{CO}_2$  reduction products, *i.e.*, formate) were replaced with new solutions. This procedure was used to verify the reproducibility of the initial performance after five hours of continuous tests.

The cumulative production of formate, carbon monoxide and hydrogen during these two cycles of 5 h is shown in Fig. 5. The current density profiles and cell voltages during irradiation time are also reported. Note that formate accumulates during the experiment, increasing the electrolyte conductivity. This fact reduces the total overpotential of the EC cell, which in turn shifts the WP to lower voltages. Since the WP is located in the steepest part of the *IV* curve, the reduction in voltage leads to a considerable increase in the measured current of the PV/EC device.

After 2 h, stable production of formate is attained, with no appearance of deactivation or loss of performance of the catalysts. Note the excellent reproducibility of the two consecutive experiments, evidencing that no relevant transformation to the electrodes occurs on these tests.

Previous electrocatalytic studies performed in the same aqueous electrolyte (0.1 M  $\text{KHCO}_3$ ) showed that the solvothermally prepared Cu-S electrocatalysts exhibited high FEs to formate (*ca.* 80% at  $-0.8$  V *vs.* RHE) and sustained their high selectivity over 12 h.<sup>29</sup> The high stability obtained in our photo-electrocatalytic tests suggests that the working potential at the cathode does not exceed  $-0.8$  V (*vs.* RHE), as also expected from the polarisation studies. On the other hand, the NiFeZn electrode provided excellent performance towards the oxygen evolution reaction and exceptional stability in 1 M KOH, as shown by supplementary experimentation reported in Section S5 in the ESI.<sup>†</sup>

Similarly, the current density increases in the first 2–3 h of each cycle, reaching stable and constant values of around  $16\text{--}17\text{ mA cm}^{-2}$  (cell voltage: 2.5 V). The FE to formate was close to 60%, similar to the values obtained in the electrochemical validation tests.

Using the data obtained from this validation test, we can describe the evolution of the working points of the device, starting from a cell voltage of around 2.7 V and finally stabilising at 2.5 V, as described by the blue triangles on the plot in Fig. 4.

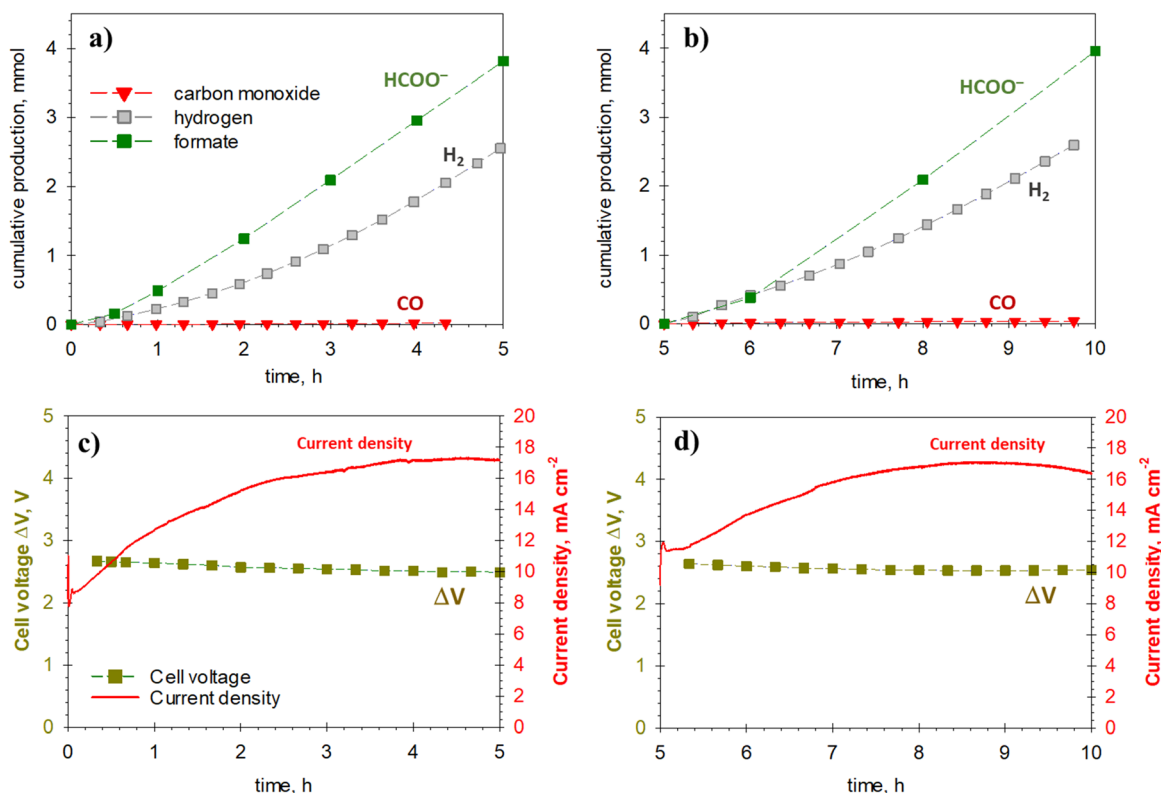
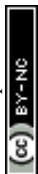


Fig. 5 Performances of the electrochemical device after coupling with the photovoltaic module. (a) Cumulative production of formate ( $\text{HCOO}^-$ ), carbon monoxide (CO) and hydrogen ( $\text{H}_2$ ) in 5 h of solar irradiation and (b) in the subsequent 5 h of irradiation. (c) Profiles of current density and cell voltage during the first 5 h and (d) during the next 5 h.





### 3.5 Solar-to-fuel (STF) efficiency

We calculated the device's photoconversion efficiency to evaluate the system's effective capability to store solar energy. Before testing the device, the solar simulator was carefully calibrated to provide a collimated output beam simulating the solar standard terrestrial irradiation (*i.e.*, 1 Sun, 100 mW cm<sup>-2</sup>). The artificial leaf works at a current density  $j = 17.3 \pm 0.5$  mA cm<sup>-2</sup>, with a cell potential of 2.5 V ( $V_{WP}$ ) and an electrode area of  $A_e = 5.31 \pm 0.05$  (cm<sup>2</sup>). With these parameters, we can estimate the ratio of solar to electrical power conversion (*i.e.*, the photovoltaic conversion efficiency) as:

$$\text{Solar-to-electricity}(\%) = \frac{V_{WP} \times j \times A_e}{P \times A_{PV}} \times 100 = 18.1\% \quad (5)$$

where  $P$  is the incident irradiation power (in W cm<sup>-2</sup>), and  $A_{PV}$  is the irradiated surface area of the PV module (in cm<sup>2</sup>), accounting for the solar irradiation power. Thus, the PV/EC setup is only losing around 2% of energy, mainly due to the slight deviation of the WP from the MPP (2.5 vs. 2.3 V) and partially to electrical connections and formation of interfaces since 18% of the solar energy is driving the electrochemical reaction. The deviation of the WP from the MPP is typically quantified as a coupling factor or coupling efficiency, which is a ratio of the WP power to the power at the MPP.

Fig. 6 shows the coupling factor *versus* time for the 10 h validation test, evidencing the evolution of the coupling factor until reaching a value of approximately 0.914 in both the two 5 h experimental runs. This increase in the coupling factor is related to the shift of the working voltage in the direction of the MPP discussed in the previous section. By multiplying the efficiency of the PV module at the MPP (19.74%) and the coupling factor (0.914), we can easily calculate the solar-to-electricity efficiency (18.04%), which is consistent with the calculation made in eqn (5), confirming that the major losses refer to the coupling loss.

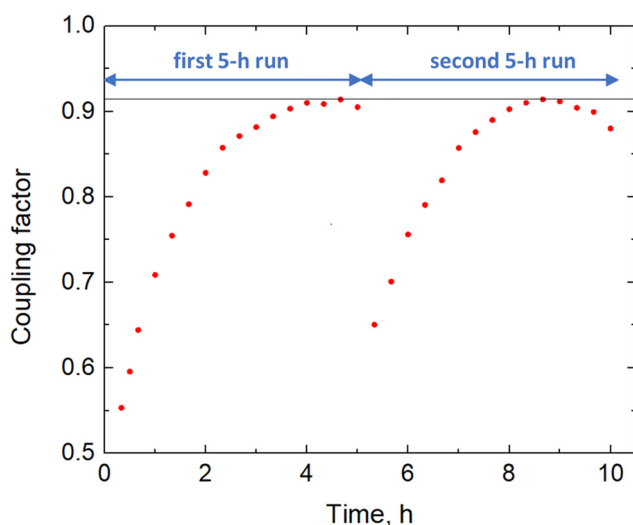


Fig. 6 Coupling factor by integrating the electrochemical device and the photovoltaic module. Coupling factor for the two 5 h experimental runs of the validation test.

Taking into account the fuel production, we can further estimate the solar-to-fuel (STF) energy efficiency with the equation:

$$\text{STF}_i(\%) = \frac{E_i \times j \times A_e \times \text{FE}_i}{P \times A_{PV}} \times 100 \quad (6)$$

where  $E_i$  corresponds to the energy stored in each product  $i$ :  $E_{\text{formate}} = 1.43$  V and  $E_{\text{hydrogen}} = 1.23$  V, and  $\text{FE}_i$  is the Faradaic efficiency to the  $i$ -reduction product.

The STF efficiency to formate is calculated as  $6.2 \pm 0.4\%$ , representing a record for a wired stand-alone artificial leaf using only non-critical raw materials and without applying external bias or adding sacrificial donors. The additional STF efficiency to hydrogen, as collected from the gas chamber, is  $3.9 \pm 0.3\%$ . The overall STF efficiency combining these two major products is  $10.1 \pm 0.5\%$ , accounting for about 99.5% of the Faradaic efficiency. Other minor products are CO (around 0.3%), formaldehyde and C2+, which appeared as traces and could not be adequately quantified.

A performance comparison of different artificial leaf-type systems reported in the literature is presented in Fig. 7. The plot reports the main results of the current density as a function of the STF efficiencies in CO<sub>2</sub> reduction processes to formate.

The data used to build the plot in Fig. 7 are summarised in Table 2, reporting selected literature results<sup>16–19,36–43</sup> for comparison with the data presented here.

Among the works not using critical raw materials and operating under relevant conditions, we obtained the maximum STF efficiency to formate (*i.e.*, 6.2%) or to combined formate + H<sub>2</sub> (*i.e.*, 10.1%). Note that Zhao *et al.*<sup>36</sup> reported a higher efficiency. Still, they worked under conditions very far from those that should be adopted for practical implementation (current density of about 1.3 mA cm<sup>-2</sup>, geometrical electrode surface area = 1 cm<sup>2</sup>). Compared to state of the art, it is also relevant to mention that the remarkable STF performance

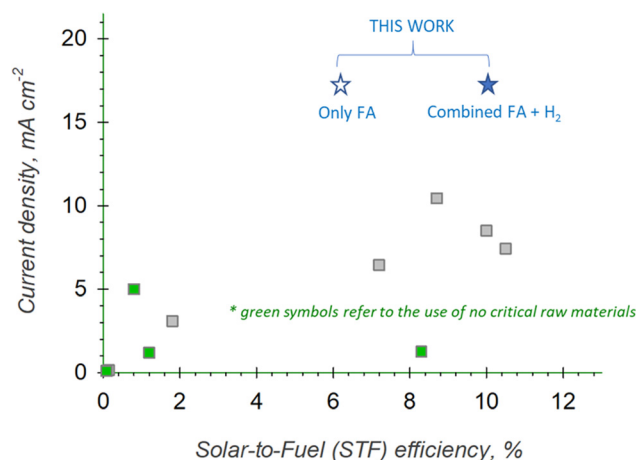


Fig. 7 Comparison of the results of artificial leaves in the literature. Current density vs. STF efficiency in CO<sub>2</sub> reduction processes to formate obtained in artificial leaf-type systems. "FA" refers to the formate, while the green squares refer to artificial leaves not using critical raw materials.



**Table 2** Summary of the main artificial leaf-type systems reported in the literature for CO<sub>2</sub> reduction, including catalysts, operating conditions and performance in terms of solar-to-fuel (STF) efficiency

Catalysts	Critical raw materials?	Cell configuration	Electrolytes	Electrode area (cm <sup>2</sup> )	Current density (mA cm <sup>-2</sup> )	Operating voltage	Faradaic selectivity to formate (%)	Formate production rate (μmol h <sup>-1</sup> cm <sup>-2</sup> )	STF (%)	Ref.
Cathode: Cu-S(GDL); anode NiFeZn oxide on GDL	No	Wired	CO <sub>2</sub> -saturated 0.1 M KHCO <sub>3</sub> aqueous solution (pH = 6.6) as catholyte; 1 M KOH aqueous solution (pH > 13)	5.3	17.3	Cell voltage = 2.5 V	59.7	192.68	6.2 (10.1 cumulative formate + H <sub>2</sub> )	This work
RuO <sub>2</sub> catalysts onto a Au layer, with SrTiO <sub>3</sub> :La,Rh and BiVO <sub>4</sub> :Mo light absorbers modified by phosphonated Co(ii) bis(terpyridine)	Yes	Wireless	CO <sub>2</sub> -saturated KHCO <sub>3</sub> aqueous solution (0.1 M, pH = 6.7)	~1	0.11	+0.45 V vs. RHE	83.9 ± 5.8%	1.088	0.08 ± 0.01	Wang <i>et al.</i> 2020 <sup>16</sup>
Pd/C nanoparticle-coated Ti mesh cathode; tandem GaAs/InGaP/TiO <sub>2</sub> /Ni photoanode	Yes	Wireless	2.8 M KHCO <sub>3(aq)</sub> (pH = 8.0) as catholyte; 1.0 MKOH <sub>(aq)</sub> (pH = 13.7) as anolyte	0.03–0.04	8.5	Cathode exhibited <100 mV overpotential; cell voltage = 2.04 V	> 94%	149.1	~10%	Zhou <i>et al.</i> 2016 <sup>17</sup>
Porous Bi dendrite electrodes synthesised on Cu substrates as cathode, IrO <sub>2</sub> anode	Yes	Wired	CO <sub>2</sub> -saturated 1 M KHCO <sub>3</sub> aqueous solution as electrolyte (only the catholyte promoted with 0.1 M CsCl)	1.2–1.6	10.46	Cell voltage = 2.7 V	~95%	125	8.7	Piao <i>et al.</i> 2020 <sup>18</sup>
Cathode: Ti/graphite/CS/MWCNTs/RuCP, anode: FTO/Ag/IrO <sub>x</sub>	Yes	Wired	0.4 M KPi (single compartment)	973	6.44 ± 0.04	Cell voltage = 1.85 V	80	96.1	7.2 ± 0.18	Kato <i>et al.</i> 2021 <sup>19</sup>
Cathode: Ti/graphite/CS/MWCNTs/RuCP, anode: Ti/IrO <sub>x</sub>	Yes	Wired	0.4 M KPi (single compartment)	8760	7.42	Cell voltage = 1.65–1.69 V	96.0	133.2	10.5	Kato <i>et al.</i> 2021 <sup>20</sup>
BiOI–Bi (BOI–Bi) cathode; argon-treated TiO <sub>2</sub> (TiO <sub>2</sub> –Ar) photoanode	No	Wired	CO <sub>2</sub> -saturated 0.5 M KHCO <sub>3</sub> aqueous solution (pH = 7.3) as catholyte; Ar-saturated 0.1 M KOH aqueous solution (pH = 12.9) as anolyte	1	1.26	Cell voltage = 1.24 V	~96.5	22.68	8.3	Zhao <i>et al.</i> 2021 <sup>36</sup>
BiVO <sub>4</sub>   Perovskite  IO-TiO <sub>2</sub>   FDH tandem	No	Wireless	86 mM MOPS [3-(N-morpholino)-propane sulfonic acid], 50 mM NaHCO <sub>3</sub> , 50 mM CsCl	0.19	5	+0.4 V vs. RHE	83 ± 5	7.0	0.8	Moore <i>et al.</i> 2021 <sup>37</sup>
InP/[RuCP] semiconductor/metal-complex hybrid photo-cathode and reduced SrTiO <sub>3</sub> photoanode	Yes	Wireless	5 mL of 0.1 M NaHCO <sub>3</sub> aqueous solution mixed with phosphoric acid (pH 7.7)	0.25	0.1	–0.75 V (vs. Ag/AgCl)	71.6	1.93	0.08	Arai <i>et al.</i> 2013 <sup>38</sup>
CuFeO <sub>2</sub> and CuO mixed p-type catalysts	No	Wireless	0.1 M bicarbonate solution purged with CO <sub>2</sub>	0.25	0.8–1.2	+0.9 V vs. RHE, cell voltage = 0.22 V	> 90	10.0	0.7–1.2	Kang <i>et al.</i> 2015 <sup>39</sup>
Cathode: N <sub>2</sub> Zn–Fe <sub>2</sub> O <sub>3</sub> on TiO <sub>2</sub> overlayer and a Cr <sub>2</sub> O <sub>3</sub> underlayer, with Ru complex (Ru(MeCN)(CO) <sub>2</sub> C <sub>3</sub> Py) deposited; photoanode: n-SrTiO <sub>3</sub>	Yes	Wireless	CO <sub>2</sub> -saturated 0.1 M KHCO <sub>3</sub> electrolyte (pH 6.6)	1	0.15	Application of 0.1 V vs. RHE	~80	0.04	0.15	Sekizawa <i>et al.</i> 2018 <sup>40</sup>



Table 2 (continued)

Catalysts	Critical raw materials?	Cell configuration	Electrolytes	Electrode area (cm <sup>2</sup> )	Current density (mA cm <sup>-2</sup> )	Operating voltage	Faradaic selectivity to formate (%)	Formate production rate (μmol h <sup>-1</sup> cm <sup>-2</sup> )	STF (%)	Ref.
3D TiN nanoshells ClFDH Bioelectrode	No	Wireless	CO <sub>2</sub> -saturated phosphate buffer (pH 6.5, 50 mM bicarbonate purged with CO <sub>2</sub> )	0.5	0.0916	−0.8 V vs. Ag/AgCl)	83.1	2.12	0.08	Kuk <i>et al.</i> 2019 <sup>41</sup>
Cathode: indium-based electrocatalyst coating deposited on a 3D Cu mesh; anode: metal Ti folded screen with an iridium oxide electrocatalyst coating	Yes	Wired	Catholyte: 1 M potassium bicarbonate; anolyte: 1 M H <sub>2</sub> SO <sub>4</sub> (95–98%)	3200	2.5–3.1	Cell voltage = 3.7 V	67	0.0938	1.8	White <i>et al.</i> 2014 <sup>42</sup>
An amorphous Si-Ge triple junction (3jn-SiGe) as a light absorber, a Ru polymer (RuCP) coated on a carbon cloth as cathode, and IrO <sub>x</sub> as anode	Yes	Wireless	CO <sub>2</sub> -saturated aqueous phosphate buffer (0.1 M K <sub>2</sub> HPO <sub>4</sub> + KH <sub>2</sub> PO <sub>4</sub> ), pH = 6.4	4	No current reported	−0.18 V vs. RHE	No FE reported	~3.8	4.6	Morikawa <i>et al.</i> 2021 <sup>43</sup>

of our device is measured at a very high current density, *i.e.*, 17.3 mA cm<sup>-2</sup>, which is the maximum value ever reported, not only considering the works involving earth-abundant materials. The formate productivity reaches about 0.19 mmol h<sup>-1</sup> cm<sup>-2</sup>, which is 45% higher than the world-record results recently obtained by Toyota<sup>20,44</sup> using noble metal-based electrodes ( $\sim 0.13$  mmol h<sup>-1</sup> cm<sup>-2</sup>, FE to formate =  $\sim 96\%$ ).

### 3.6 Technology assessment

Fig. 8 reports the simplified scheme of the technology of combined production of formate (used as a hydrogen storage molecule) and H<sub>2</sub>. The flowsheet reports the quantitative data (in grams per day, assuming 1 m<sup>2</sup> of the PV panel and 7.4 h of solar illumination per day, which is the annual average value in Sicily – Italy). By balancing the direct H<sub>2</sub> production and that deriving from formate decomposition (when sunlight is not present) and using a small intermediate vessel to store H<sub>2</sub>, a continuous (24 h) production of H<sub>2</sub> of about 2 g h<sup>-1</sup> per m<sup>2</sup> of the PV panel can be obtained. In this simplified scheme, 100% FE to formate + H<sub>2</sub> has been assumed. Although we experimentally observed the formation of low amounts of CO (as well as of other minor by-products), we believe that further optimisation of the system (acting both on the electrocatalyst formulation and operating conditions) can reduce these by-products to a non-critical level. Eventually, CO can be removed by the established PROX (Preferential Oxidation) method, which can efficiently be performed over metal catalysts of the platinum group (modified with promoters like alkali metals or reducible metal oxides) operating at low temperatures in the presence of water and CO<sub>2</sub>,<sup>45</sup> or also over earth-abundant material-based catalysts like copper oxide–cerium oxide, in which the high selectivity can be related to the preferential adsorption of CO on Cu<sup>+</sup> active sites hindering H<sub>2</sub> dissociation.<sup>46</sup>

Based on this quantitative scheme, some assessment considerations can be made. The first question is with regard to the

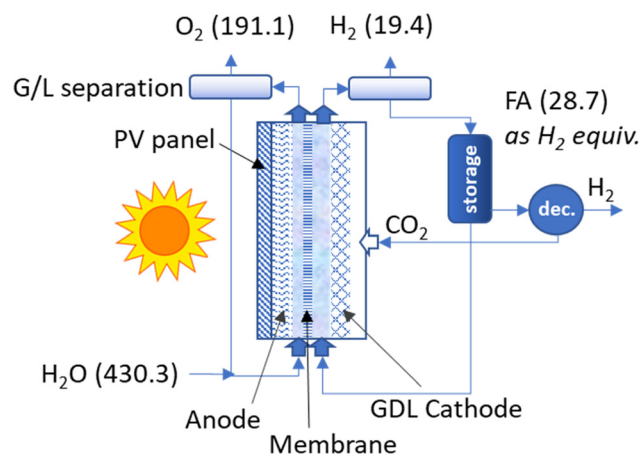


Fig. 8 Simplified quantitative flowsheet of the technology for the combined formate and H<sub>2</sub> production on the PV/EC cell, with quantitative data in grams per m<sup>2</sup> of the PV panel and day (assuming 7.4 h a day of sunlight). "dec." indicates a stage of catalytic decomposition of formate (FA) to CO<sub>2</sub> and H<sub>2</sub>.

often-raised issue of the impact of green  $\text{H}_2$  production on water. The amount by weight of water feed to  $\text{H}_2$  produced is around 9, corresponding to the ratio between the molecular weights. The difference is the produced  $\text{O}_2$  because the atom efficiency of the reaction is 100%. The use of  $\text{H}_2$  will form  $\text{H}_2\text{O}$  again. Thus, it is not essentially water consumption but a transfer of solar energy to the form of chemical energy (*i.e.*,  $\text{H}_2$ ) that can be used as a clean fuel or reactant. While a more comprehensive life-cycle assessment (LCA) would be required, we do not see the impact of this technology on water as a critical issue. In contrast, the production of fuels and chemicals from fossil resources often has a higher impact on water on LCA bases.

The other point emerging from Fig. 8 is that in the presented concept of formate +  $\text{H}_2$  combined production,  $\text{CO}_2$  will be fully recycled, except for the tiniest part going to other C-based products (however, the C-selectivity to formate can be further improved as discussed above). Thus, this technology is not designed to use  $\text{CO}_2$  to reduce its emission directly but to produce ultra-low carbon (green)  $\text{H}_2$ , bypassing the discontinuity in solar light availability. The key element is a technology integrating the production of  $\text{H}_2$  and an  $\text{H}_2$ -storage compound that can form hydrogen during dark periods. This is a novel concept in the area of green  $\text{H}_2$  production.

The proposed technology will overcome the downstream separation process to obtain pure FA (usually performed by distillation or extraction methods).<sup>22</sup> In fact, separating FA from the electrolyte is unnecessary, as it can be directly used in catalytic decomposition to produce  $\text{H}_2$  without separation. The decomposition of FA is an already established process, usually performed in reactors using both homogeneous and heterogeneous catalysts.<sup>47</sup> The fixed bed reactor is the most common and more studied reactor for FA decomposition. For example, Koós and Solymosi<sup>48</sup> reported the catalytic activity of  $\text{Mo}_2\text{C}$  catalysts in the vapour-phase using a continuous flow fixed bed reactor. Under the conditions adopted for the experimental tests,  $\text{Mo}_2\text{C}$  is an effective catalyst for the dehydrogenation of FA to yield  $\text{H}_2$  and  $\text{CO}_2$ . Still, it competes with the FA dehydration reaction to yield  $\text{H}_2\text{O}$  and  $\text{CO}$ . However, the authors observed that adding water to FA eliminated  $\text{CO}$  formation giving a  $\text{CO}$ -free  $\text{H}_2$  stream. Thus, the presence of water can even be beneficial for this process step, making the separation of FA from the electrolyte unnecessary.

Moreover, the authors obtained the best results by working with an aqueous solution of FA (5–6%). Considering that our artificial leaf-type system allows the production of FA at a rate of  $\sim 8 \text{ mg cm}^{-2} \text{ h}^{-1}$ , it is easy to reveal that we can reach the desired FA concentration in about 8–10 h, which precisely refers to the period time of our validation tests (and also approximately to the time of sunlight irradiation per day). Note that a careful techno-economic assessment (TEA) would be required to validate this technology.

Our preliminary calculations, based on experimentation with our lab-scale device, show that the combined production of formate and  $\text{H}_2$  can provide a continuous and constant  $\text{H}_2$  productivity that, although relatively low, could be used for

decentralised production of  $\text{H}_2$  to cover domestic needs. Further improvements in the performance of the PV/EC device are possible, *i.e.* the solar-to-fuel efficiency may be enhanced to 15%, or the FE to formate to 80%, but this will not essentially increase the daily productivity of  $\text{H}_2$ . The main parameter affecting this value is the current density. The methods to improve it at the level necessary for exploitability are (i) integrating the PV module with other external electrical energy sources (wind-powered, for example) or (ii) using solar concentrators to enhance SUN irradiation (tests here are made with one SUN).

There are various relatively cheap solutions to have a SUN concentration in the 5–100 SUN range (one SUN indicates the irradiance of one solar constant), which could be integrated into the device. A SUN concentration in the 10–20 range could improve the  $\text{H}_2$  productivity while limiting overheating of the device. Note also that with the availability of higher current densities, the design of the EC part (including synthesis of the electrocatalytic materials, electrode engineering and optimisation of the operating conditions) should be adapted to be coupled with PV modules working at higher light irradiation/current density (to operate close to the MPP).

We also remark that our AL presents many advantages concerning analogous systems that instead produce  $\text{CO}$ . As discussed above, we realised a device based on only earth-abundant materials with top-level performance (as reported in Fig. 7). In contrast, most other literature results are based on using noble and costly metals for  $\text{CO}$  formation. For example, Cheng *et al.*<sup>49</sup> valuably reported the performance of a solar-driven gas diffusion electrode flow cell with a solar-to-fuel conversion efficiency of 19.1%. They used a gas diffusion electrode employing an Ag nanoparticle catalyst layer for  $\text{CO}_2$  reduction in their PEC cell wired with a GaInP/GaInAs/Ge triple-junction photovoltaic cell. The availability of all these materials is considered to be at serious risk within 100 years.<sup>50</sup> We demonstrate that it is possible to achieve high performance even without these elements. In addition, they used very small electrodes and PV cells (with a geometrical area of  $\sim 0.3 \text{ cm}^2$ ). The size of our electrodes and PV cell is much larger (almost  $6 \text{ cm}^2$  and  $13 \text{ cm}^2$ , respectively), thus more than one order of magnitude higher. Although small demonstrations are of fundamental importance, especially in the first step of the investigation, there are aspects related to mass transfer and charge diffusion not taken into account with low electrode areas. The size of the electrodes/devices is an issue of paramount importance in determining the needed cell voltage for additional overpotential phenomena along the surface of the electrodes that increase with the geometrical area. Moreover, it is more challenging to prepare uniformly larger electrodes, which should be taken into strong consideration in scaling up the fabrication of the electrodes. Lab results obtained with very low geometrical surface areas are insufficient to prove the concept and analyse the system's scalability.

Furthermore, the thermodynamic potential needed for the reduction of  $\text{CO}_2$  to  $\text{CO}$  is more favourable than the reduction potential to FA ( $-0.53 \text{ V}$  against  $-0.61 \text{ V}$ , respectively).<sup>51</sup> Our AL produces FA and no  $\text{CO}$  ( $\text{CO}$  formation was very low and may be





easily reduced at zero, as discussed above). Apart from the importance of making selectively FA (which is a liquid product that can be completely separated from the hydrogen gas produced), FA is a more valuable product than CO. Carbon monoxide might be considered as a fuel, but when downstream converted in combination with H<sub>2</sub> (with the further issue to control the CO:H<sub>2</sub> ratio depending on the process). In contrast, FA is a base material for several industries and is considered a promising hydrogen carrier or energy carrier for direct fuel cell power. It is more challenging to obtain FA than CO, as the reaction mechanism for FA formation involves the introduction of H atoms in the CO<sub>2</sub> molecule after selective activation of the latter, although the mechanistic aspects still need to be clarified. Thus, the selective formation of FA is not only a matter of catalyst, but other aspects, such as the diffusion of H species towards the electrode surface, can play a fundamental role. Recently, some of us studied the influence of proton diffusion in the liquid- and gas-phase, highlighting the importance of cell/electrode design and operating conditions in addressing the selectivity of CO<sub>2</sub> reduction beyond the properties of the electrocatalysts themselves.<sup>52</sup> The design of our AL considers all these phenomena, which can favour the production of FA and H<sub>2</sub> in place of CO.

Our AL device uses different electrolytes in cathode and anode compartments because the two electrodes (Cu-S and Ni-Fe-Zn oxide) are stable and work efficiently at different pHs. In general, the pH in the electrolyte solutions can vary for (i) crossover of ions and/or (ii) consumption of H<sup>+</sup> and OH<sup>-</sup> needed for the half-reactions (CO<sub>2</sub>RR and OER, respectively). In our case, we observed that, in the period of tests (*i.e.* ten hours), the PTFE-reinforced Nafion allowed maintaining the initial pH difference during the electrocatalytic tests (pH variation to only 0.2 points, with an analytical error of  $\pm 0.07$ ), also limiting the crossover of ions (as usually observed from standard thin Nafion or anion exchange membranes).

However, the pH variation may become important for more extended operations, and recycling the catholyte and anolyte solutions in an auxiliary process is demanding if no counter-measures are taken. The most helpful strategy is the adoption of a bipolar exchange membrane, which offers stable local pH values by hindering cations and anions from passing through the membrane and supplying H<sup>+</sup> to the cathode and OH<sup>-</sup> to the anode for water dissociation at the interface layer of the membrane<sup>11</sup> (see also Section S3 in the ESI<sup>†</sup>). Of course, in the case of bipolar membranes, acid-base neutralisation should be considered in the economy of the process.<sup>53</sup>

Regarding energy efficiency, the solar-to-fuel value of the proposed device is about 10%, which can be only slightly reduced from the downstream units illustrated in Fig. 8. A direct comparison of this efficiency with a conventional electrolyser (with green electrical energy supplied by a PV field and a storage unit for electrical energy storage to allow 24 h continuous operations) may only have limited meaning. This technology aims to develop AL devices, which may lead to artificial trees that produce H<sub>2</sub> for domestic uses. Thus, the integration of the elements is a must, despite the absolute

efficiency. Solar light itself is not a reactant having a cost. Nevertheless, we can indicate that the energy efficiency of the integrated system reported in Fig. 8 can be a cost-effective and efficient technology advantageous to the current state of the art<sup>54–56</sup> when further developed.

## 4. Conclusions

In summary, we have demonstrated that the combination of an electrochemical (EC) cell and a photovoltaic (PV) module in a wired configuration, exclusively built with earth-abundant and non-critical raw materials, is a suitable option for reducing energy losses, reaching a high efficiency (*i.e.*, 6.2% to formate or 10.1% to combined H<sub>2</sub> + formate) and for storing solar energy as formate with productivity  $> 8 \text{ mg cm}^{-2} \text{ h}^{-1}$  by CO<sub>2</sub> electroreduction. This achievement was realised by optimised electrode development and adjusted and accurate integration of all parts and components to minimise losses. Furthermore, the PV module and the EC cell were designed to offer a correct matching to operate at the best working point.<sup>57</sup> Additional reductions of the overvoltage of the two half-cell reactions (CO<sub>2</sub> reduction and oxygen evolution reactions) will lead to even higher performance values.

Our device was validated for over ten hours without observing any deactivation of the electrocatalytic materials (in both the cathode and anode), providing high stability during the solar irradiation tests.

The device is proposed to produce ultra-low carbon (green) H<sub>2</sub> with an integrated system to store hydrogen as formate, which can then decompose to produce H<sub>2</sub>, providing a continuous daily H<sub>2</sub> production of  $2 \text{ g h}^{-1} \text{ per m}^2$  of the PV panel. This solution realises better-integrated AL devices with advantages over non-integrated systems, particularly for an objective to move to future artificial-tree systems for domestic production of H<sub>2</sub>. Although the H<sub>2</sub> productivity is relatively low, its constant continuous output can be used for decentralised energy production, but a careful TEA analysis is necessary to validate this technology. Alternatively, the device could produce chemicals (formate) by CO<sub>2</sub> electro-conversion; in this case, further improvements are needed to increase the FE to formate.

In both cases, scaling up the electrode surface area (*e.g.*, to  $\geq 500 \text{ cm}^2$ ) will be required to implement this device. Furthermore, additional efforts are needed in the manufacturing processes for integration, such as (i) lower cathodic and anodic overpotential, (ii) more extended stability tests, (iii) lower cathodic pH to produce formic acid instead of formate, to enable the implementation of affordable artificial leaves.

In addition, the technology proposed here overcomes the problem of discontinuity in the production of H<sub>2</sub> by devices using (only) renewable electrical energy because it integrates a solution for efficient intermediate hydrogen storage. Only the AL-type device was tested here because the other elements of the overall scheme presented in Fig. 8 are already established. At the same time, the discussion evidences some directions to explore for moving to application.



In conclusion, it is helpful to remark on the breakthrough advances presented in this work:

1. We report world top-level results regarding solar-to-fuel efficiency and current density, as shown in Fig. 7. The combined solar-to-fuel efficiency is 10% (to FA and H<sub>2</sub>), a value still often presented at conferences as a target for future research. Although recent papers reported good results in terms of STF efficiency higher or close to 10% at reasonable current density, it is essential to remark that indicating only the solar-to-fuel efficiency, as often reported in the literature, is misleading because high STF efficiency values can be obtained under conditions that are not relevant in terms of productivity (current density). From this perspective, this paper represents a breakthrough in achieving top-level results considering current density and solar-to-fuel efficiency.

2. We demonstrate for the first time the feasibility of producing with a PV-EC device a continuous production of H<sub>2</sub> (24 h) *via* the coproduction of an H<sub>2</sub>-storage molecule (formate – FA) which can be decomposed during dark operations (with recycling of CO<sub>2</sub>) to allow the continuous production of H<sub>2</sub>. This concept is entirely original and presented for the first time, representing another breakthrough element opening new directions and overcoming the issues related to using PEC devices only when solar light is present, thus a fraction of the day.

3. We realised a device based on earth-abundant materials with top-level performance, while most of the other literature results are based on using noble and costly metals, such as Ir, Ru, *etc.* We demonstrate that high performance can be achieved even without these elements.

Many efforts have been devoted to integrating all the elements constituting the artificial leaf (electrocatalytic materials, substrates, membranes, PV module, *etc.*). Although their main characteristics and individual behaviours were already known, the resulting performance in a full device could be very low without proper integration of the main pieces. An optimal WP was obtained from coupling the EC device with the PV cell (see Fig. 4), which was very close to the maximum power point and defined suitable working conditions (in terms of the current–potential couple) to provide high FEs to the target products.

Other systems in the literature reported high STF efficiency but working at relatively low current density, as the latter depends on integrating the EC device with the PV cell. We would also like to remark that the current density (specific to the target products) is the main parameter to consider from the implementation point of view, as it is directly proportional to the process yield/productivity.

The realisation of the artificial leaf was made possible thanks to multidisciplinary scientific work involving top-level research institutions and universities participating in this work within the funded European A-LEAF Project,<sup>23</sup> each focusing on optimising a specific aspect/component of the artificial leaf.

The work has introduced many novel aspects of the production of solar fuels, which have been critically discussed here. The paper has also highlighted the main issues of these types of systems (such as the need to maintain the pH difference

between the two half-cells of the EC device), which can stimulate further research to find new technological solutions and make the implementation of artificial leaves economically affordable.

## 5. Experimental

### 5.1 Synthesis of Cu-S

Copper sulfide (Cu-S) was prepared by adapting a solvothermal method reported elsewhere.<sup>58,59</sup> Briefly, four mmol of Cu(NO<sub>3</sub>)<sub>2</sub>·3H<sub>2</sub>O and 0.067 mmol of elemental sulfur (Sigma-Aldrich, >95%) were mixed in 40 mL of ethylene glycol (Sigma-Aldrich, 99%) under stirring at room temperature for 30 min. The mixture, transferred into a 50 mL Teflon-lined autoclave, was heat-treated at 140 °C for ten hours (with a heating rate of 5 °C min<sup>-1</sup>), and finally cooled at room temperature. The resulting mixture was washed with ultrapure water three times by centrifugation (6000 rpm, 10 min), and the obtained powder was dried under vacuum overnight at 80 °C.

### 5.2 Synthesis of Ni-Zn-Fe oxide

The metal oxide NiZnFeO<sub>x</sub> was obtained *via* a hydrothermal method. Equimolecular amounts of metal nitrates were dissolved in water (metal concentration: 50 mM), and the solution was hydrolysed with diluted aqueous ammonia until pH = 8.5 was achieved. The solution was introduced into a Teflon cup and mounted in an autoclave at 140 °C for 2 h. After the hydrothermal treatment, the pressure vessel was cooled in air, the product was washed with H<sub>2</sub>O and CH<sub>3</sub>CH<sub>2</sub>OH, and the nanoparticles were collected by centrifugation (final particle size: ~8 nm).

### 5.3 Electrode preparation

Cu-S (or Ni-Fe-Zn oxide) powders were deposited on carbon-based substrates to prepare the electrodes. In detail, a weighted amount of catalyst (to obtain a final loading of 1.0 mg cm<sup>-2</sup>) was mixed with 4 mL of water and 4 mL of isopropanol and 50 µL of 10% Nafion<sup>®</sup> perfluorate and sonicated until the formation of a stable suspension (15 min). The resulting ink was deposited by spray coating onto a pre-heated porous carbon-based gas-diffusion layer (GDL, Sigracet<sup>®</sup> 39BCE, supplied by Ion Power), acting as the support, allowing the evaporation of the solvent and fixing the powder uniformly on the electrode surface.

### 5.4 Electrochemical device

The electrochemical setup is described in Section 2. The Plexiglas cell has a highly compact configuration. The two GDEs (the cathode with Cu-S and the anode with Ni-Fe-Zn oxide) were located within the electrochemical cell, with the catalyst facing the liquid phase. The geometrical surface area of both electrodes is about 5.3 cm<sup>2</sup>. A 3 M Ag/AgCl capillary electrode (1 mm dia., supplied by Alvaltek) was used as the reference electrode and located very close to the working electrode to minimise overpotential. The potential values were



then translated into RHE (Reversible Hydrogen Electrode) voltages by using the following equation:

$$E_{(\text{RHE})} = E_{\text{Ag/AgCl}} + 0.059 \text{ pH} + 0.21 \quad (7)$$

Continuous recirculation of the catholyte and anolyte between each half-cell (cathode and anode, respectively) and two independent reservoir containers was performed using a peristaltic pump working at a liquid flow rate of  $50 \text{ mL min}^{-1}$ .

$20 \text{ mL min}^{-1}$  of pure  $\text{CO}_2$  was flowed into the catholyte reservoir (in connection with the cathode compartment of the cell) to saturate the  $\text{KHCO}_3$  solution. At the equilibrium, a pH of 6.78 was reached in the catholyte before starting the electrochemical tests. Other  $20 \text{ mL min}^{-1}$  of pure  $\text{CO}_2$  also flowed into the gas chamber.

A potentiostat/galvanostat (Autolab PGSTAT204 with FRA32M Module, supplied by Metrohm) was used to perform the electrochemical characterisation.

Gaseous products from the cathode outlet stream ( $\text{H}_2$ ,  $\text{CH}_4$ ,  $\text{CO}$ ,  $\text{C}_2\text{H}_4$ , and  $\text{C}_2\text{H}_6$ ) were detected using a Gas Chromatograph (MicroGC GCX Pollution Analytic Equipment), having a sensitivity of 1–2 ppm, by sampling from the cathodic reservoir every 20 min. The liquid catholyte was analysed by Ion Chromatography (IC Metrohm 940 Professional, column Metrohm Organic Acids) to detect the presence of liquid products such as formate (and eventually acetate and oxalate). The presence of other liquid products (*i.e.*, methanol, ethanol, methyl formate, and acetone) was checked by Gas Chromatography-Mass Spectrometry (GC-MS Thermo 1310-Tsq 8000 Evo, column Stabilwax).

## Author contributions

This paper derives from a joint EU project (A-LEAF) where the partners (a) developed the cell, the partners (b) the PV module, the partners (c) and (d) the electrocatalytic components and the partners (e) and (f) to the analysis of the results. The manuscript was designed and written by CA in collaboration with GC, with the contribution of all other authors.

## Conflicts of interest

There are no conflicts to declare.

## Acknowledgements

The European Union funded this work through the H2020-FETPROACT Project Number 732840 titled “An Artificial Leaf: a photo-electro-catalytic cell from earth-abundant materials for sustainable solar production of  $\text{CO}_2$ -based chemicals and fuels (A-LEAF)”, which is gratefully acknowledged. TM, VS, UC and OA would also like to thank the silicon heterojunction solar cell baseline; Alain Doumit for the wafer texture and cleaning; Silke Lynen, Volker Lauterbach, and Andreas Mück for PECVD deposition; Hildegard Siekmann for the ITO sputtering; Sunny Peris for module encapsulation; and Dr Kaining Ding,

Dr Andreas Lambertz and Dr Weiyuan Duan for scientific support. Additional sources of funding were the European Union through the DECADE H2020 project (ID: 862030) and the MIUR (Italy) through the PRIN Project  $\text{CO}_2$  ONLY (No. 2017WR2LRS), acknowledged by CA, DG, MM, GC and SP, and ETH Zurich through an ETH Research Grant (ETH-47 19-1), acknowledged by FLPV. SG also acknowledges support from the project PID2020-116093RB-C41 funded by MCIN/AEI/10.13039/501100011033.

## References

- 1 X. Li, J. Yu, M. Jaroniec and X. Chen, Cocatalysts for Selective Photoreduction of  $\text{CO}_2$  into Solar Fuels, *Chem. Rev.*, 2019, **119**, 3962–4179, DOI: [10.1021/acs.chemrev.8b00400](https://doi.org/10.1021/acs.chemrev.8b00400).
- 2 C. Ampelli, G. Centi, R. Passalacqua and S. Perathoner, Synthesis of solar fuels by a novel photoelectrocatalytic approach, *Energy Environ. Sci.*, 2010, **3**, 292–301, DOI: [10.1039/b925470f](https://doi.org/10.1039/b925470f).
- 3 J. R. Galán-Mascarós, Photoelectrochemical solar fuels from carbon dioxide, water and sunlight, *Catal. Sci. Technol.*, 2020, **10**, 1967–1974, DOI: [10.1039/c9cy02606a](https://doi.org/10.1039/c9cy02606a).
- 4 A. J. Martín and J. Pérez-Ramírez, Heading to Distributed Electrocatalytic Conversion of Small Abundant Molecules into Fuels, Chemicals, and Fertilizers, *Joule*, 2019, **3**, 2602–2621, DOI: [10.1016/j.joule.2019.09.007](https://doi.org/10.1016/j.joule.2019.09.007).
- 5 D. K. Dogutan and D. G. Nocera, Artificial Photosynthesis at Efficiencies Greatly Exceeding That of Natural Photosynthesis, *Acc. Chem. Res.*, 2019, **52**, 3143–3148, DOI: [10.1021/acs.accounts.9b00380](https://doi.org/10.1021/acs.accounts.9b00380).
- 6 COM(2020) 474-Critical Raw Materials Resilience: Charting a Path towards greater Security and Sustainability, European Commission, 2020, <https://ec.europa.eu/docsroom/documents/42849/attachments/2/translations/en/renditions/native>.
- 7 T. Wang and J. Gong, Sacrificing nothing to reduce  $\text{CO}_2$ , *Nat. Energy*, 2020, **5**, 642–643, DOI: [10.1038/s41560-020-00688-3](https://doi.org/10.1038/s41560-020-00688-3).
- 8 O. Khaselev and J. A. Turner, A Monolithic Photovoltaic-Photoelectrochemical Device for Hydrogen Production via Water Splitting, *Science*, 1998, **280**, 425–427, DOI: [10.1126/science.280.5362.425](https://doi.org/10.1126/science.280.5362.425).
- 9 S. Y. Reece, J. A. Hamel, K. Sung, T. D. Jarvi, A. J. Esswein, J. J. H. Pijpers and D. G. Nocera, Wireless Solar Water Splitting Using Silicon-Based Semiconductors and Earth-Abundant Catalysts, *Science*, 2011, **334**, 645–648, DOI: [10.1126/science.1209816](https://doi.org/10.1126/science.1209816).
- 10 A. Kumar, V. Hasija, A. Sudhaik, P. Raizada, Q. Van Le, P. Singh, T.-H. Pham, T. Y. Kim, S. Ghotekar and V.-H. Nguyen, Artificial leaf for light-driven  $\text{CO}_2$  reduction: Basic concepts, advanced structures and selective solar-to-chemical products, *Chem. Eng. J.*, 2022, **430**, 133031, DOI: [10.1016/j.cej.2021.133031](https://doi.org/10.1016/j.cej.2021.133031).



- 11 F. Urbain, P. Tang, N. M. Carretero, T. Andreu, L. G. Gerling, C. Voz, J. Arbiol and J. Ramon Morante, A prototype reactor for highly selective solar-driven CO<sub>2</sub> reduction to synthesis gas using nanosized earth-abundant catalysts and silicon photovoltaics, *Energy Environ. Sci.*, 2017, **10**, 2256–2266, DOI: [10.1039/c7ee01747b](https://doi.org/10.1039/c7ee01747b).
- 12 M. Zhang, W. Wei, S. Zhou, D.-D. Ma, A. Cao, X.-T. Wu and Q.-L. Zhu, Engineering a conductive network of atomically thin bismuthine with rich defects enables CO<sub>2</sub> reduction to formate with industry-compatible current densities and stability, *Energy Environ. Sci.*, 2021, **14**, 4998–5008, DOI: [10.1039/d1ee01495a](https://doi.org/10.1039/d1ee01495a).
- 13 S. A. Al-Tamreh, M. H. Ibrahim, M. H. El-Naas, J. Vaes, D. Pant, A. Benamor and A. Amhamed, Electroreduction of Carbon Dioxide into Formate: A Comprehensive Review, *ChemElectroChem*, 2021, **8**, 3207–3220, DOI: [10.1002/celec.202100438](https://doi.org/10.1002/celec.202100438).
- 14 R. van Putten, T. Wissink, T. Swinkels and E. A. Pidko, Fuelling the hydrogen economy: Scale-up of an integrated formic acid-to-power system, *Int. J. Hydrog. Energy*, 2019, **44**, 28533–28541, DOI: [10.1016/j.ijhydene.2019.01.153](https://doi.org/10.1016/j.ijhydene.2019.01.153).
- 15 J. Eppinger and K.-W. Huang, Formic Acid as a Hydrogen Energy Carrier, *ACS Energy Lett.*, 2017, **2**, 188–195, DOI: [10.1021/acsenenergylett.6b00574](https://doi.org/10.1021/acsenenergylett.6b00574).
- 16 Q. Wang, J. Warnan, S. Rodríguez-Jiménez, J. J. Leung, S. Kalathil, V. Andrei, K. Domen and E. Reisner, Molecularly engineered photocatalyst sheet for scalable solar formate production from carbon dioxide and water, *Nat. Energy*, 2020, **5**, 703–710, DOI: [10.1038/s41560-020-0678-6](https://doi.org/10.1038/s41560-020-0678-6).
- 17 X. Zhou, R. Liu, K. Sun, Y. Chen, E. Verlage, S. A. Francis, N. S. Lewis and C. Xiang, Solar-Driven Reduction of 1 atm of CO<sub>2</sub> to Formate at 10% Energy-Conversion Efficiency by Use of a TiO<sub>2</sub>-Protected III–V Tandem Photoanode in Conjunction with a Bipolar Membrane and a Pd/C Cathode, *ACS Energy Lett.*, 2016, **1**, 764–770, DOI: [10.1021/acsenenergylett.6b00317](https://doi.org/10.1021/acsenenergylett.6b00317).
- 18 G. Piao, S. H. Yoon, D. S. Han and H. Park, Ion-Enhanced Conversion of CO<sub>2</sub> into Formate on Porous Dendritic Bismuth Electrodes with High Efficiency and Durability, *ChemSusChem*, 2020, **13**, 698–706, DOI: [10.1002/cssc.201902581](https://doi.org/10.1002/cssc.201902581).
- 19 N. Kato, S. Mizuno, M. Shiozawa, N. Nojiri, Y. Kawai, K. Fukumoto, T. Morikawa and Y. Takeda, A large-sized cell for solar-driven CO<sub>2</sub> conversion with a solar-to-formate conversion efficiency of 7.2%, *Joule*, 2021, **5**, 687–705, DOI: [10.1016/j.joule.2021.01.002](https://doi.org/10.1016/j.joule.2021.01.002).
- 20 N. Kato, Y. Takeda, Y. Kawai, N. Nojiri, M. Shiozawa, S. Mizuno, K.-I. Yamanaka, T. Morikawa and T. Hamaguchi, Solar Fuel Production from CO<sub>2</sub> Using a 1 m-Square-Sized Reactor with a Solar-to-Formate Conversion Efficiency of 10.5%, *ACS Sustainable Chem. Eng.*, 2021, **9**, 16031–16037, DOI: [10.1021/acssuschemeng.1c06390](https://doi.org/10.1021/acssuschemeng.1c06390).
- 21 V. Romano, G. D'Angelo, S. Perathoner and G. Centi, Current density in solar fuel technologies, *Energy Environ. Sci.*, 2021, **14**, 5760–5787, DOI: [10.1039/d1ee02512k](https://doi.org/10.1039/d1ee02512k).
- 22 M. Ramdin, A. R. T. Morrison, M. de Groen, R. van Haperen, R. de Kler, E. Irtem, A. T. Laitinen, L. J. P. van den Broeke, T. Breugelmans, J. P. M. Trusler, W. de Jong and T. J. H. Vlugt, High-Pressure Electrochemical Reduction of CO<sub>2</sub> to Formic Acid/Formate: Effect of pH on the Downstream Separation Process and Economics, *Ind. Eng. Chem. Res.*, 2019, **58**, 22718–22740, DOI: [10.1021/acs.iecr.9b03970](https://doi.org/10.1021/acs.iecr.9b03970).
- 23 H2020-EU.1.2.2.-FET Proactive, “An Artificial Leaf: a photo-electro-catalytic cell from earth-abundant materials for sustainable solar production of CO<sub>2</sub>-based chemicals and fuels”, Grant agreement 732840-A-LEAF, <https://www.a-leaf.eu/>.
- 24 N. Lazouski, M. Chung, K. Williams, M. L. Gala and K. Manthiram, Non-aqueous gas diffusion electrodes for rapid ammonia synthesis from nitrogen and water-splitting-derived hydrogen, *Nat. Catal.*, 2020, **3**, 463–469, DOI: [10.1038/s41929-020-0455-8](https://doi.org/10.1038/s41929-020-0455-8).
- 25 C. Ampelli, Electrode design for ammonia synthesis, *Nat. Catal.*, 2020, **3**, 420–421, DOI: [10.1038/s41929-020-0461-x](https://doi.org/10.1038/s41929-020-0461-x).
- 26 W. Duan, A. Lambertz, K. Bittkau, D. Qiu, K. Qiu, U. Rau and K. Ding, A route towards high-efficiency silicon heterojunction solar cells, *Prog. Photovolt. Res. Appl.*, 2022, **30**, 384–392, DOI: [10.1002/pip.3493](https://doi.org/10.1002/pip.3493).
- 27 M. Lee, X. Ding, S. Banerjee, F. Krause, V. Smirnov, O. Astakhov, T. Merdzhanova, B. Klingebiel, T. Kirchartz, F. Finger, U. Rau and S. Haas, Bifunctional CoFeVO<sub>x</sub> Catalyst for Solar Water Splitting by using Multijunction and Heterojunction Silicon, *Solar Cells, Adv. Mater. Technol.*, 2020, **5**, 2000592, DOI: [10.1002/admt.202000592](https://doi.org/10.1002/admt.202000592).
- 28 J. Yu, P. S. Leonard, D. Qiu, Y. Zhao, A. Lambertz, C. Zahren, L. Volker, W. Duan, J. Yu and K. Ding, Light-induced performance of SHJ solar modules under 2000 h illumination, *Sol. Energy Mater. Sol. Cells*, 2022, **235**, 111459, DOI: [10.1016/j.solmat.2021.111459](https://doi.org/10.1016/j.solmat.2021.111459).
- 29 T. Shinagawa, G. O. Larrazábal, A. J. Martín, F. Krumeich and J. Pérez-Ramírez, Sulfur-Modified Copper Catalysts for the Electrochemical Reduction of Carbon Dioxide to Formate, *ACS Catal.*, 2018, **8**, 837–844, DOI: [10.1021/acscatal.7b03161](https://doi.org/10.1021/acscatal.7b03161).
- 30 S. Nitopi, E. Bertheussen, S. B. Scott, X. Liu, A. K. Engstfeld, S. Horch, B. Seger, I. E. L. Stephens, K. Chan, C. Hahn, J. K. Nørskov, T. F. Jaramillo and I. Chorkendorff, Progress and Perspectives of Electrochemical CO<sub>2</sub> Reduction on Copper in Aqueous Electrolyte, *Chem. Rev.*, 2019, **119**, 7610–7672, DOI: [10.1021/acs.chemrev.8b00705](https://doi.org/10.1021/acs.chemrev.8b00705).
- 31 D. Giusi, C. Ampelli, C. Genovese, S. Perathoner and G. Centi, A novel gas flow-through photocatalytic reactor based on copper-functionalized nanomembranes for the photoreduction of CO<sub>2</sub> to C1–C2 carboxylic acids and C1–C3 alcohols, *Chem. Eng. J.*, 2021, **408**, 127250, DOI: [10.1016/j.cej.2020.127250](https://doi.org/10.1016/j.cej.2020.127250).
- 32 F. A. Garcés-Pineda, H. C. Nguyễn, M. Blasco-Ahicart, M. García-Tecedor, M. de Fez Febré, P.-Y. Tang, J. Arbiol, S. Giménez, J. R. Galán-Mascarós and N. López, Push-Pull Electronic Effects in Surface-Active Sites Enhance Electrocatalytic Oxygen Evolution on Transition Metal Oxides, *ChemSusChem*, 2021, **14**, 1595–1601, DOI: [10.1002/cssc.202002782](https://doi.org/10.1002/cssc.202002782).
- 33 B. Turan, J.-P. Becker, F. Urbain, F. Finger, U. Rau and S. Haas, Upscaling of integrated photoelectrochemical water-splitting





- devices to large areas, *Nat. Commun.*, 2016, 7, 12681, DOI: [10.1038/ncomms12681](https://doi.org/10.1038/ncomms12681).
- 34 J.-P. Becker, B. Turan, V. Smirnov, K. Welter, F. Urbain, J. Wolff, S. Haas and F. Finger, A modular device for large area integrated photoelectrochemical water-splitting as a versatile tool to evaluate photoabsorbers and catalysts, *J. Mater. Chem. A*, 2017, 5, 4818–4826, DOI: [10.1039/c6ta10688a](https://doi.org/10.1039/c6ta10688a).
  - 35 M. Lee, B. Turan, J.-P. Becker, K. Welter, B. Klingebiel, E. Neumann, Y. J. Sohn, T. Merdzhanova, T. Kirchartz, F. Finger, U. Rau, S. Haas and A. Bias-Free, Stand-Alone, and Scalable Photovoltaic–Electrochemical Device for Solar Hydrogen Production, *Adv. Sustainable Syst.*, 2020, 4, 2000070, DOI: [10.1002/advsu.202000070](https://doi.org/10.1002/advsu.202000070).
  - 36 J. Zhao, L. Xue, Z. Niu, L. Huang, Y. Hou, Z. Zhang, R. Yuan, Z. Ding, X. Fu, X. Lu and J. Long, Conversion of CO<sub>2</sub> to formic acid by integrated all-solar-driven artificial photosynthetic system, *J. Power Sources*, 2021, 512, 230532, DOI: [10.1016/j.jpowsour.2021.230532](https://doi.org/10.1016/j.jpowsour.2021.230532).
  - 37 E. E. Moore, V. Andrei, A. R. Oliveira, A. M. Coito, I. A. C. Pereira and E. Reisner, A Semi-artificial Photoelectrochemical Tandem Leaf with a CO<sub>2</sub>-to Formate Efficiency Approaching 1%, *Angew. Chem., Int. Ed.*, 2021, 60(50), 26303–26307, DOI: [10.1002/anie.202110867](https://doi.org/10.1002/anie.202110867).
  - 38 T. Arai, S. Sato, T. Kajino and T. Morikawa, Solar CO<sub>2</sub> reduction using H<sub>2</sub>O by a semiconductor/metal-complex hybrid photocatalyst: enhanced efficiency and demonstration of a wireless system using SrTiO<sub>3</sub> photoanodes, *Energy Environ. Sci.*, 2013, 6, 1274–1282, DOI: [10.1039/c3ee24317f](https://doi.org/10.1039/c3ee24317f).
  - 39 U. Kang, S. K. Choi, D. J. Ham, S. M. Ji, W. Choi, D. S. Han, A. Abdel-Wahabe and H. Park, Photosynthesis of formate from CO<sub>2</sub> and water at 1% energy efficiency via copper iron oxide catalysis, *Energy Environ. Sci.*, 2015, 8, 2638–2643, DOI: [10.1039/C5EE01410G](https://doi.org/10.1039/C5EE01410G).
  - 40 K. Sekizawa, S. Sato, T. Arai and T. Morikawa, Solar-Driven Photocatalytic CO<sub>2</sub> Reduction in Water Utilizing a Ruthenium Complex Catalyst on p-Type Fe<sub>2</sub>O<sub>3</sub> with a Multiheterojunction, *ACS Catal.*, 2018, 8, 1405–1416, DOI: [10.1021/acscatal.7b03244](https://doi.org/10.1021/acscatal.7b03244).
  - 41 S. K. Kuk, Y. Ham, K. Gopinath, P. Boonmongkolras, Y. Lee, Y. W. Lee, S. Kondaveeti, C. Ahn, B. Shin, J.-K. Lee, S. Jeon and C. B. Park, Continuous 3D Titanium Nitride Nanoshell Structure for Solar-Driven Unbiased Biocatalytic CO<sub>2</sub> Reduction, *Adv. Energy Mater.*, 2019, 9, 1900029, DOI: [10.1002/aenm.201900029](https://doi.org/10.1002/aenm.201900029).
  - 42 J. L. White, J. T. Herb, J. J. Kaczur, P. W. Majsztrik and A. B. Bocarsly, Photons to formate: Efficient electrochemical solar energy conversion via reduction of carbon dioxide, *J. CO<sub>2</sub> Util.*, 2014, 7, 1–5, DOI: [10.1016/j.jcou.2014.05.002](https://doi.org/10.1016/j.jcou.2014.05.002).
  - 43 T. Morikawa, S. Sato, K. Sekizawa, T. M. Suzuki and T. Arai, Solar-Driven CO<sub>2</sub> Reduction Using a Semiconductor/Molecule Hybrid Photosystem: From Photocatalysts to a Monolithic Artificial Leaf, *Acc. Chem. Res.*, 2022, 55, 933–943, DOI: [10.1021/acs.accounts.1c00564](https://doi.org/10.1021/acs.accounts.1c00564).
  - 44 Toyota Central R&D Labs, A new leaf unfolds in artificial photosynthesis, Advertisement Feature, Nature Research Custom Media, 2021.
  - 45 K. Liu, A. Wang and T. Zhang, Recent Advances in Preferential Oxidation of CO Reaction over Platinum Group Metal Catalysts, *ACS Catal.*, 2012, 2, 1165–1178, DOI: [10.1021/cs200418w](https://doi.org/10.1021/cs200418w).
  - 46 A. Davó-Quinóner, M. Navlani-García, D. Lozano-Castelló, A. Bueno-López and J. A. Anderson, Role of Hydroxyl Groups in the Preferential Oxidation of CO over Copper Oxide–Cerium Oxide Catalysts, *ACS Catal.*, 2016, 6, 1723–1731, DOI: [10.1021/acscatal.5b02741](https://doi.org/10.1021/acscatal.5b02741).
  - 47 S. Hafeez, E. Harkou, A. Spanou, S. M. Al-Salem, A. Villa, N. Dimitratos, G. Manos and A. Constantinou, Review on recent progress and reactor setups for hydrogen production from formic acid decomposition, *Mater. Today Chem.*, 2022, 26, 101120, DOI: [10.1016/j.mtchem.2022.101120](https://doi.org/10.1016/j.mtchem.2022.101120).
  - 48 A. Koós and F. Solymosi, Production of CO-Free H<sub>2</sub> by Formic Acid Decomposition over Mo<sub>2</sub>C/Carbon Catalysts, *Catal. Lett.*, 2010, 138, 23–27, DOI: [10.1007/s10562-010-0375-3](https://doi.org/10.1007/s10562-010-0375-3).
  - 49 W.-H. Cheng, M. H. Richter, I. Sullivan, D. M. Larson, C. Xiang, B. S. Brunschwig and H. A. Atwater, CO<sub>2</sub> Reduction to CO with 19% Efficiency in a Solar-Driven Gas Diffusion Electrode Flow Cell under Outdoor Solar Illumination, *ACS Energy Lett.*, 2020, 5, 470–476, DOI: [10.1021/acsenerylett.9b02576](https://doi.org/10.1021/acsenerylett.9b02576).
  - 50 <https://ec.europa.eu/docsroom/documents/42849/attachments/2/translations/en/renditions/native>.
  - 51 Z. Lang, J. Miao, Y. Lan, J. Cheng, X. Xu and C. Cheng, Polyoxometalates as electron and proton reservoir assist electrochemical CO<sub>2</sub> reduction, *APL Mater.*, 2020, 8, 120702, DOI: [10.1063/5.0031374](https://doi.org/10.1063/5.0031374).
  - 52 D. Giusi, M. Miceli, C. Genovese, G. Centi, S. Perathoner and C. Ampelli, In situ electrochemical characterization of Cu<sub>x</sub>O-based gas-diffusion electrodes (GDEs) for CO<sub>2</sub> electrocatalytic reduction in presence and absence of liquid electrolyte and relationship with C<sub>2</sub><sup>+</sup> products formation, *Appl. Catal. B*, 2022, 2022318, 121845, DOI: [10.1016/j.apcatb.2022.121845](https://doi.org/10.1016/j.apcatb.2022.121845).
  - 53 Z. M. Bhat, D. Pandit, S. Ardo, R. Thimmappa, A. R. Kottaichamy, N. C. Dargily, M. C. Devendrachari and M. O. Thotiyil, An Electrochemical Neutralization Cell for Spontaneous Water Desalination, *Joule*, 2020, 4, 1730–1742, DOI: [10.1016/j.joule.2020.07.001](https://doi.org/10.1016/j.joule.2020.07.001).
  - 54 H. L. Tuller, Solar to fuels conversion technologies: a perspective, *Mater. Renew. Sustain. Energy*, 2017, 6, 3, DOI: [10.1007/s40243-017-0088-2](https://doi.org/10.1007/s40243-017-0088-2).
  - 55 J. A. Herron, J. Kim, A. A. Upadhye, G. W. Huber and C. T. Maravelias, A general framework for the assessment of solar fuel technologies, *Energy Environ. Sci.*, 2015, 8, 126–157, DOI: [10.1039/C4EE01958J](https://doi.org/10.1039/C4EE01958J).
  - 56 S. Fukuzumi, Production of Liquid Solar Fuels and Their Use in Fuel Cells, *Joule*, 2017, 1, 689–738, DOI: [10.1016/j.joule.2017.07.007](https://doi.org/10.1016/j.joule.2017.07.007).
  - 57 O. Astakhov, V. Smirnov, U. Rau and T. Merdzhanova, Prediction of Limits of Solar-to-Hydrogen Efficiency from Polarisation Curves of the Electrochemical Cells, *Sol. RRL*, 2022, 6, 2100783, DOI: [10.1002/solr.202100783](https://doi.org/10.1002/solr.202100783).



- 58 G. O. Larrazábal, A. J. Martín, F. Krumeich, R. Hauert and J. Pérez-Ramírez, Solvothermally-Prepared Cu<sub>2</sub>O Electrocatalysts for CO<sub>2</sub> Reduction with Tunable Selectivity by the Introduction of p-Block Elements, *ChemSusChem*, 2017, **10**, 1255–1265, DOI: [10.1002/cssc.201601578](https://doi.org/10.1002/cssc.201601578).
- 59 C. Wu, S.-H. Yu and M. Antonietti, Complex Concaved Cuboctahedrons of Copper Sulfide Crystals with Highly Geometrical Symmetry Created by a Solution Process, *Chem. Mater.*, 2006, **18**, 3599–3601, DOI: [10.1021/cm060956u](https://doi.org/10.1021/cm060956u).

